Response to reviewer #1

We thank the reviewer for the constructive comments and suggestions, which are very positive to improve scientific content of the manuscript. We have revised the manuscript appropriately and addressed all the reviewer's comments point-by-point for consideration as below. The remarks from the reviewer are shown in black, and our responses are shown in blue color. All the page and line numbers mentioned following are refer to the revised manuscript without change tracked.

1. The novelty of this paper is the inclusion of ground-based observations, but I think the ground-based measurements are underused in this study. Since a main part of this study is on HCHO, I don't see how the authors use ground-based measurements of HCHO to support satellite HCHO. Do you see similar temporal patterns from ground vs. space? This may also help understand the difference between column vs. surface HCHO.

R: Thanks for the constructive comments. The ground surface HCHO has been measured by LP-DOAS at the Jiangwan campus of Fudan University in Shanghai (31.34 °N, 121.52 °E) during 2018-2019 to compare with satellite observation. In order to match ground-based and spaced observations for comparison, the satellite HCHO within 10 km of LP-DOAS measurement site were averaged as the satellite observation, while the surface HCHO observed by LP-DOAS between 13:00 and 14:00 were used considering the OMI overpasses time.

Figure R1 shows that HCHO VCDs and surface HCHO concentrations are not consistent very well. For daily observation, two observations are quite different, but the monthly averages are more similar. However, the difference still exists, for example, the highest value of HCHO VCD in 2019 appeared in June, while that of surface observations appeared in August. It also suggests that the FNR from satellite will deviate from the surface observed FNR.

It should be noticed that the vertical column density represents the concentration of the total column, while the LP-DOAS results only reflect the concentration near the ground. Previous studies show that HCHO is not completely concentrated near the ground, but has a high concentration at higher altitudes (Chan et al., 2019; Wang et al., 2019). It may explain the discrepancy of tropospheric HCHO VCD observed by satellite and the ground surface HCHO concentration. In addition, satellite data reflects the average level of a given area, while LP-DOAS is a single point measurement. The spatial heterogeneity of surface HCHO concentration in horizontal can also impact the consistency of this comparison.

We have also added the comparison between satellite and surface HCHO in the manuscript, please refer to Line 130-134.

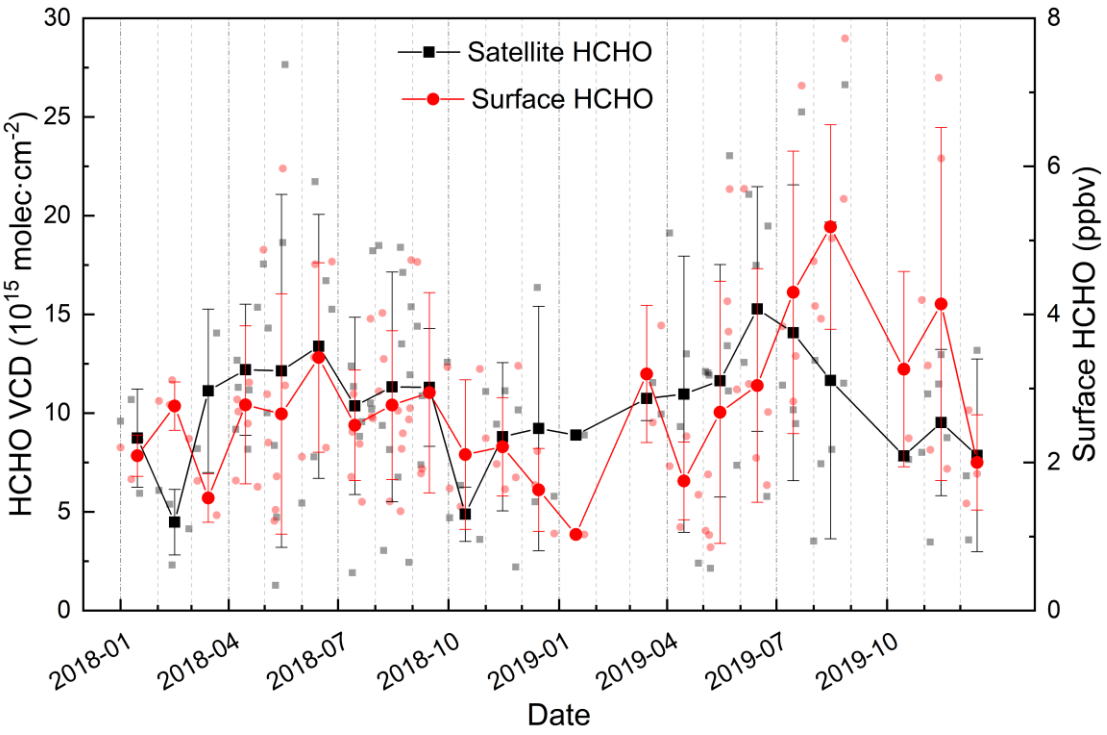

Figure R1. Comparison of daily and monthly HCHO observed by LP-DOAS and satellite. The black and red points represent the daily HCHO VCD and surface HCHO respectively, while the dot lines indicate the monthly averages.

2. There seems to be some artificial strip patterns with HCHO (Figure 2), which looks like due to the influence of OMI swath changes. It is not clear how the authors process OMI HCHO data. The authors mentioned they re-grid the data to 0.01°× 0.01°, which is much finer than the resolution of OMI. No details are provided in terms of spatial downscaling. In general, spatial oversampling is used to process OMI data to achieve better resolution (e.g. Zhu et al., 2014). I suggest the authors consider following such procedure.

R: Thanks for your professional comments. In this study, OMI HCHO data were processed through the following steps. Firstly, the targeted area was gridded into to a spatial resolution of 0.01°×0.01°, then the HCHO VCD of each pixel was assigned to the respective grid by determining the coordinates information. In addition, a weight function including cloud function and pixel size was introduced to effectively improve the quality of processed data (Xue et al., 2020). We have supplemented the data processing method in the revised manuscript, please refer to Line 89-91.

We have carefully reviewed the recommended article, as well as the articles that used the same strategy (Fioletov et al., 2011; McLinden et al., 2012; Zhu et al., 2014). In these studies, pixel falling within a certain radius of the grid center were averaged, and further was assigned to that grid. Then, the differences on HCHO VCDs between these two methods were compared. Three years, i.e. 2010, 2014 and 2018, were selected randomly for test, as shown in Figure R2. HCHO VCDs in Shanghai obtained by these two methods were almost the same in annual average. Most areas show similar HCHO levels, and about 84.6% ± 1.1% area of Shanghai shows the difference between the two

methods within 10%. Considering the different approaches in satellite data processing, such a level of difference is considered to be reasonable and accepted.

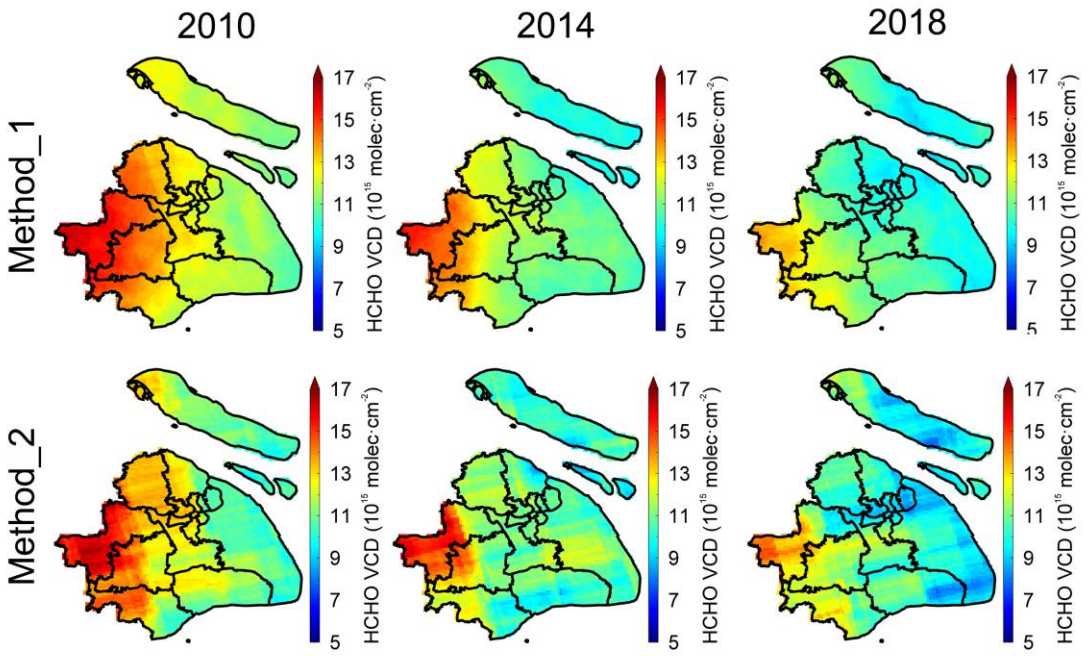

Figure R2. Comparison of the spatial distribution of HCHO VCD in Shanghai for 2010, 2014 and 2018 obtained by these two processing methods. Method_1 represents the method recommended by the references, Method_2 represents the method used in this study.

It can be noticed that there are strip patterns in the spatial distribution of HCHO VCD via Methond_2 in Figure R2 (also appeared in Figure 2), which not appear in the one via Methond_1. The absence of smoothing procedure in Method_2 may be the main reason causing the difference in the results of these two methods. After the improvements in the algorithm of OMI HCHO Version 3.0, across-track striping of the HCHO columns is a minor issue of the new satellite product (https://aura.gesdisc.eosdis.nasa.gov/data/Aura_OMI_Level2/OMHCHO.003/doc/README.OMHCHO.pdf). So the strip patterns in the spatial distribution of HCHO VCD are considered not introduced by artificial processing, but inherited due to unsmoothing in Method_2.

3. It's not clear to me how the authors explore the impacts of anthropogenic emissions on HCHO. There seems to be several issues. First, the authors only consider the primary emissions of HCHO, but a lot of HCHO is produced secondarily from other VOCs like alkene. The HCHO yield should also vary with VOC species, and also meteorology. Second, as I pointed out earlier, the authors did not consider the role of biogenic emissions especially isoprene. Without secondary HCHO, there is little we can learn about the driven factors of HCHO from this paper.

R: Thank you for the professional comments. Secondary production of HCHO from anthropogenic and biogenic sources has contributed greatly to HCHO, so it is necessary to consider the secondary production of HCHO (Zhu et al., 2017; Shen et al., 2019).

We have also considered the secondary production of HCHO in the revised manuscript, including anthropogenic and biogenic sources. Please refer to Line 176-205.

In order to get the secondary production of HCHO from anthropogenic sources, NMVOCs (Non-methane volatile organic compounds) emission inventory based on the SAPRC07 mechanism species from Multi-resolution Emission Inventory for China (MEIC) was used for years of 2010, 2012, 2014 and 2016. Secondary production of HCHO has been calculated based on 1-day HCHO yields of several NMVOCs under high-NO_x condition (Shen et al., 2019). Table R1 summarizes the primary emissions and secondary productions of HCHO from different sectors of anthropogenic sources.

Table R1. The primary emissions and estimated secondary productions of HCHO in Shanghai from anthropogenic NMVOCs based on SAPRC07 mechanism species.

Year		Estimated HCHO production from each sector (10^9 g)				
		Industry	Power	Residential	Transportation	Total
2010	Primary[1]	9.10	0.03	0.06	1.47	10.66
	Secondary[2]	240.58	0.52	15.14	66.04	322.28
2012	Primary	7.73	0.05	0.07	1.01	8.86
	Secondary	246.67	0.57	15.67	51.91	314.82
2014	Primary	6.88	0.05	0.07	0.74	7.74
	Secondary	253.32	0.50	16.44	44.32	314.58
2016	Primary	6.29	0.05	0.06	0.61	7.01
	Secondary	286.36	0.51	16.64	43.14	346.65

[1] Primary indicates HCHO that is directly emitted by anthropogenic sources from MEIC inventory.

[2] Secondary indicates HCHO that is produced by anthropogenic NMVOCs, which is calculated based on 1-day HCHO yields.

Regardless of the primary emissions or secondary productions of HCHO, industry sector corresponds to the largest yield, followed by transportation, residential, and the power. For the temporal pattern, the primary emission of HCHO keeps decreasing (about 34.2% compared to 2010), while secondary produced HCHO did not change significantly. The increase of secondary HCHO yields in 2016 was mainly due to the increased production from industry sector. In addition, the changes and proportional relationships between primary emission and secondary production of HCHO for different sectors are different, which suggests the VOCs source profiles of different sectors would affect the amount of secondary HCHO production.

In addition, considering the mechanism species for different chemical mechanisms in MEIC inventory may have impacts on HCHO secondary production, we have also tested the HCHO yields based on CB05 mechanism species. HCHO yields in eastern China during May-September 2010 were calculated based on CB05 and SAPRC07 separately, and results were compared with the study of Shen et al. (2019). As shown in Table R2, total HCHO yield based on CB05 is about 23% higher than that of SAPRC07, and the latter is much closer to the reference, with a deviation of 7.1%. The

high degree of lumping of PAR in CB05 may cause the corresponding individual VOC to be overestimated, and caused the large deviation of HCHO yield. Compared with CB05, SPRAC07 may be more accurate for calculating the HCHO yield. It also illustrates that the selection of chemical mechanism species would also introduce uncertainty to the estimation.

Table R2. Estimated May-September total HCHO production in eastern China in 2010 from CB05 and SAPRC07 mechanism species and the comparison with reference.

Species	Estimated HCHO production from anthropogenic NMVOCs in eastern China (Tg)		
	CB05[1]	SAPRC07	Reference[2]
Ethane	0.27	0.28	0.28
Propane	1.29	0.19	0.54
≥C4 alkanes	1.40	1.75	1.87
Ethylene	0.76	0.75	0.75
≥C3 alkenes	0.89	1.88	1.11
Benzene	0.03	0.05	0.038
Toluene	0.51	0.35	0.37
Xylenes	0.62	0.23	0.11
Formaldehyde	0.14	0.09	0.09
Acetaldehyde	0.11	0.04	0.04
Methanol	0.06	0.06	0.06
Ethanol	0.06	-	0.01
Acetone	0.90	0.15	0.16
Methy ethyl ketone	0.14	0.04	0.04
Isoprene	0.01	0.01	0
Monoterpene	0.02	0.02	0
Total	7.21	5.86	5.47

[1] Highly lumping mechanism species of CB05, including PAR, are approximately allocated through some individual VOC concentrations observed locally.

[2] Reference refer to the estimated May-September total HCHO production from Anthropogenic emission in eastern China averaged during 2005-2016 (Shen et al., 2019).

HCHO yield from biogenic sources can be estimated from BVOCs emission inventory. Model of Emissions of Gases and Aerosols from Nature (MEGAN) is widely used to simulate the emission of BVOCs. As we currently cannot use MEGAN to accurately simulate four-year (2010, 2012, 2014, 2016) BVOCs emissions, we have used the annual total BVOCs emissions of Shanghai in 2014 (about 1.2×10^4 t) for the estimation (Liu et al., 2018a; Liu et al., 2018b). Isoprene, methanol and monoterpenes were dominant compositions of BVOCs and accounted about 81.3% of the total. We have calculated HCHO yields contributed by isoprene, methanol and monoterpenes, as shown in Table R3.

Table R3. The annual BVOCs emissions and HCHO yields over Shanghai in 2014.

BVOC	Emission (10^9 g)	HCHO yield (10^9 g)
Isoprene	4.63	4.70
Methanol	4.26	3.99
Monoterpenes	0.86	0.38
Total	9.75	9.07

Accordingly, HCHO yield from BVOCs emission was estimated to be about 9.07×10^9 g, and mostly produced from isoprene and methanol. The calculated HCHO yield from BVOCs emission is similar to that of previous study during 2005-2016 (Shen et al., 2019). In addition, compared with anthropogenic sources, HCHO yield from BVOCs is much smaller, which indicates that the anthropogenic is the main contributor of the secondary production of HCHO in Shanghai (Shen et al., 2019; Fan et al., 2021).

As shown in Table R4, we have also reviewed the related studies about the BVOCs emissions in Shanghai and its surrounding areas (the Yangtze River Delta) in relevant years. Wang et al. (2021a) assessed the impacts of land cover change and climate variability on BVOCs emissions in China from 2001 to 2016, in which variations of BVOCs emissions in Shanghai over the years were extremely small. Considering the different input dataset and settings would bring large differences in the simulated results, it was unfeasible to use BVOCs emissions from different studies for the investigation of temporal variation. Therefore, the BVOCs emissions in 2014 were used to basically characterize the approximate level of BVOCs from 2010 to 2016 in this study.

Table R4. Comparison of simulated BVOCs emissions in Shanghai (SH) and the Yangtze River Delta (YRD) based on MEGAN.

Simulated year	Reference	MEGAN version	Region	BVOCs emission (10^4 t)
2010	Song et al. (2012)[1]	V 2.04	YRD	110
			SH	0.122
2014	Liu et al. (2018a; 2018b)[2]	V 2.10	YRD	188.6
			SH	1.2
2016	Wang et al. (2021b)[3]	V 3.1	YRD	162 [1]
			SH	~ 0.34 [4]

[1] Total annual emission inferred from the simulated BVOCs emissions in January, April, July and October.

[2] A variety of methods were used to reduce the uncertainty of plant functional types (PFT) database. The proportions of dominant components of BVOCs were also provided.

[3] BVOCs emission was simulated without drought stress.

[4] It is BVOCs emissions in July, which has been inferred from Fig. S3 of Wang et al. (2021b).

As mentioned in Reviewer #2, HCHO yield was also impacted by the NO_x levels, e.g. RO_2 radical from VOCs react with HO_2 to from organic peroxides under low NO_x

condition. This process reduces the reaction of RO_2 and NO, which in turn decreases the production of HCHO, therefore, HCHO yield from VOCs is proportional to NO_x condition (Palmer et al., 2006; Marais et al., 2012; Miller et al., 2017). In this study, the estimation using a fixed HCHO yield may overestimate HCHO production in later years due to the decreases of NO_x in Shanghai (Xue et al., 2020). In previous studies, the proportional relationship between HCHO yield and NO_x condition was usually obtained when 1 ppbv of NO_x regard as the high condition, and 0.1 ppbv of NO_x regard as low condition (Palmer et al., 2006; Marais et al., 2012; Miller et al., 2017). However, the NO_x concentration in Shanghai is still relatively higher (basically 30-60 ppbv in urban) (Gao et al., 2017). Therefore, in such a high NO_x condition, the effect of NO_x decreases on HCHO yield needs to be further studied.

4. Recent literature report there is uncertainty with the regime threshold for HCHO/NO2. The authors consider the uncertainty with diurnal cycle, but even at the overpass time, the regime threshold may also vary (Shroeder et al., 2017; Jin et al., 2020; Souri et al., 2020). I suggest the authors be more cautionary about applying the thresholds to separate regimes. More validation analysis is needed to support their regime classification.

R: Thank you for the professional comments. We have carefully reviewed the recommended articles. In these articles, various regime thresholds were proposed through chemical model or combining satellite result with ground surface observation, the complexity of applying the threshold is also discussed in detail (Schroeder et al., 2017; Jin et al., 2020; Souri et al., 2020). Although the O_3 formation sensitivity cannot be perfectly inferred from satellite HCHO/NO_2, this method benefits from the advantages of satellite observation and can still provide useful information on O_3 formation.

In this study, we did not obtain the new regime thresholds through such method, but used LP-DOAS data to correct the value of FNR observed by satellite. These two programs are similar in actual effect. Please refer to the following response for a detailed explanation of satellite FNR correction.

5. As I commented previously, the correction for diurnal variation doesn't make sense to me. First, the authors did not consider the difference between column-based satellite HCHO/NO2 vs. surface observed HCHO/NO2. Given the variation of the boundary layer height, the relationship between surface and column HCHO/NO2 should also vary with time. Second, it's not clear to me why the authors use ΔO3 to weight FNR. If the authors are only interested in the time when ozone production is most efficient, wouldn't it be easier to look the 1-hour maximum ozone? Third, there is no evidence supports whether such changes actually improved the regime classification.

R: Thank you for the professional comments. At the beginning, we have verified the relationship between surface FNR and O_3 during the day. As shown in Figure R3, the hourly O_3 concentration is in good agreement with surface FNR, which means that the surface FNR observed by LP-DOAS can be a good indicator of ground surface O_3 on a detailed time scale. Considering that satellites can only characterize the FNR situation

at overpass time, while LP-DOAS can provide a longer period of surface FNR variations, we hope to introduce the time series of LP-DOAS FNR to make satellite FNR be a better indicator that can reflect the characteristic of O_3 formation during the daytime.

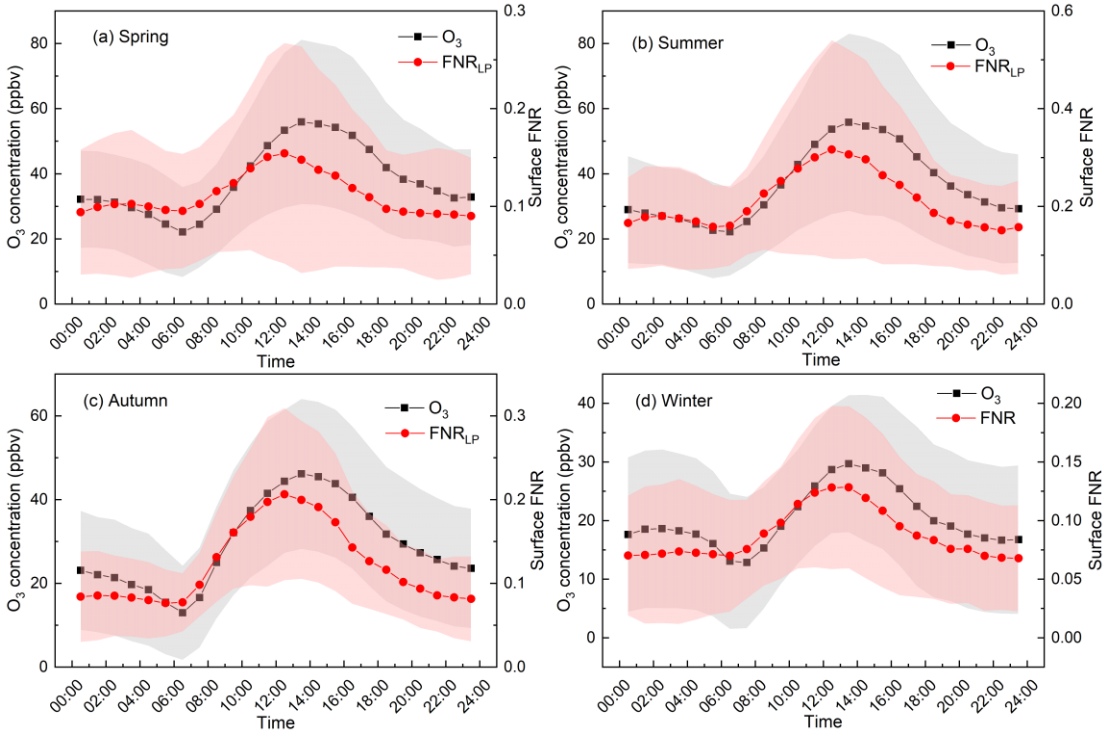

Figure R3. Diurnal variations of surface FNR observed by LP-DOAS and O_3 for different seasons during 2018-2019.

Then, we have compared the satellite FNR and surface FNR observed by LP-DOAS on daily and monthly scales, and discussed whether satellite FNR can indicate ground surface O_3 properly like LP-DOAS FNR. In the following comparison, surface FNR is observed by LP-DOAS for 13:00-14:00, satellite FNR is the average value of 10 km area around LP-DOAS measurement site.

Figure R4 shows the variation of monthly satellite and surface FNR. Since the satellite and surface FNR represent the column average and ground surface $HCHO/NO_2$ respectively, they have a significant difference in the numerical value, the satellite FNR is significantly larger than the surface FNR. However, a strong correlation between the monthly satellite and surface FNR ($R^2 = 0.95$) was found from April to August, which means that satellite FNR can characterize the O_3 formation on monthly scale like surface FNR.

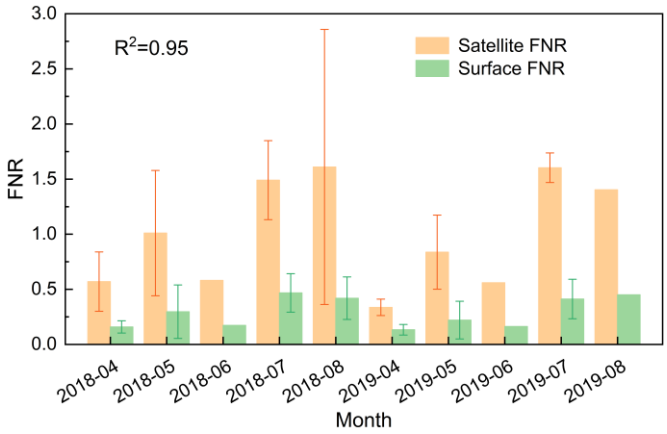

Figure R4. The variations of monthly satellite and surface FNR at the location of LP-DOAS for April to August during 2018-2019.

For the daily comparison, we have followed the suggestion to consider the influence of the boundary layer height (BLH) on the relationship between the satellite and surface FNR. The BLHs at 13:00 local time was selected to conform the overpass time of satellite. Figure R5 plotted the satellite and surface FNR under different BLHs. It indicates that on the daily scale, satellite and the surface FNR were quite different, and the relationship is affected by BLH. When the atmospheric turbulence is strong, the boundary layer is higher than 1500 m, the fitting slope of the satellite and surface FNR is small (slope=0.59, R=0.80). However, in the case of weak atmospheric turbulence, the corresponding boundary layer is lower than 1000 m, and the fitting slope of the satellite and surface FNR is large (slope=2.59, R=0.67) in this situation.

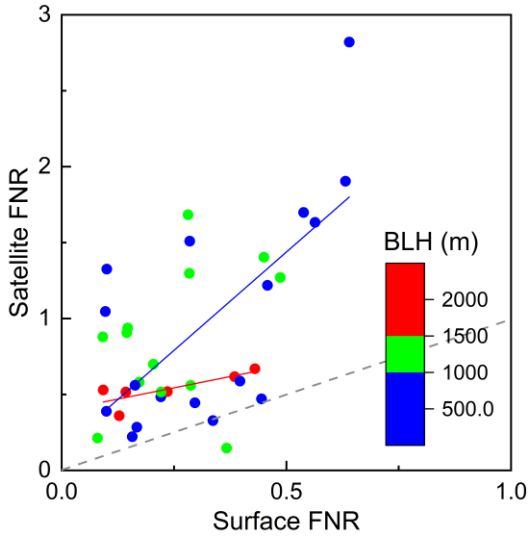

Figure R5. Satellite and surface FNR under different boundary layer heights. The gray dashed line represents y=x, the red and blue lines represent the fit of satellite and surface FNR when the BLHs greater than 1500 m and less than 1000 m respectively. The BLH data comes from the fifth generation European Centre for Medium-Range Weather Forecasts reanalysis dataset (https://cds.climate.copernicus.eu/cdsapp#!/home).

Regarding the parameter to weight FNR, we are not only interested in the time when O_3 formation is most efficient. 1-hour maximum O_3 only represents O_3 condition in a moment, which is contrary to the aim to make the corrected FNR better reflecting the temporal formation of O_3 during the daytime by introducing the time series of LP-DOAS FNR. In addition, as FNR is originally proposed as an indicator to characterize the instantaneous O_3 production rate, we used ΔO_3 as the weight to avoid the effect of O_3 accumulation (high O_3 concentration but with small increase or even decrease of O_3) (Duncan et al., 2010). Take June 5th, 2018 as an example, the 1-hour maximum O_3 in Hongkou Site was about 109.35 ppbv, while ΔO_3 was only 0.47 ppbv at that time, indicating the low efficient of O_3 formation. While from 07:00 to 12:00 that day, ΔO_3 were basically greater than 10 ppbv. Therefore, we used the hourly ΔO_3 as the weight to correct satellite FNR combined with the hourly LP-DOAS FNR.

In order to verify whether the correction of the satellite FNR improved the regime classification, we have compared the O_3 formation regimes determined by satellite FNR before and after the correction with that of surface observation. The variations of O_3 with surface HCHO and NO_2 during the daytime have been plotted to determine the O_3 formation regimes from the surface observation (Figure R6). The surface HCHO and NO_2 are from LP-DOAS measurements, and the O_3 observed by SP-DOAS (short-path differential optical absorption spectroscopy), which also located at Jiangwan campus of Fudan University, have been used with a finer temporal resolution. O_3 formation regimes inferred from satellite FNR before and after the correction have also been marked in Figure R6 separately.

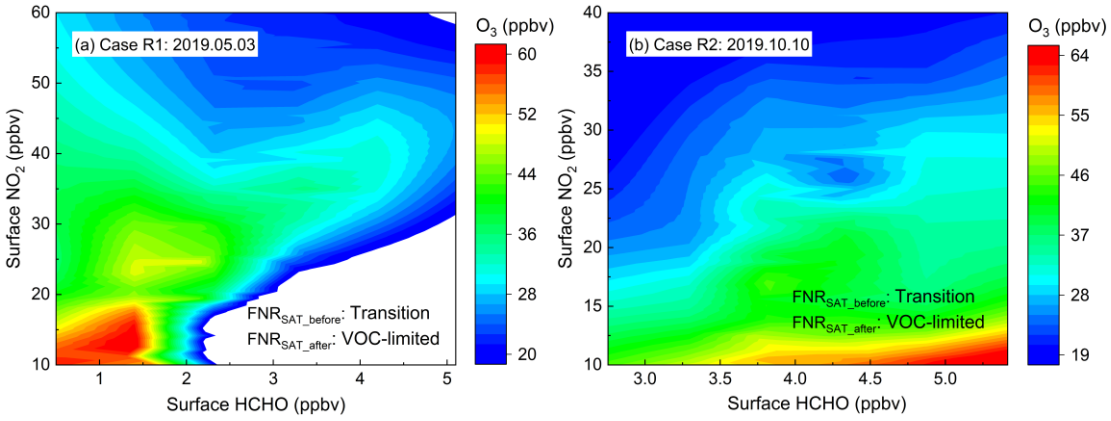

Figure R6. The variation of O_3 with surface HCHO and NO_2 for two cases of (a) May 3th, 2019 and (b) October 10th, 2019. FNR_{SAT_before} and FNR_{SAT_after} indicate the O_3 formation regimes inferred from the satellite FNR before and after the correction.

For Case R1, O_3 decreases with the increase of NO_2, which can be attributed to the titration of O_3 by NO (Duncan et al., 2010). O_3 increased from top to bottom of the diagram indicating it was under VOC-limited regime in Case R1 (Luo et al., 2020). For Case R2, it can be seen that the high O_3 appeared with high HCHO and low NO_2, indicating it was under VOC-limited regime. The uncorrected satellite FNR indicated that these two cases were both under transition regime, while the corrected satellite FNR indicated they transferred to VOC-limited regime, which are consistent with the

results of surface observation. Therefore, the correction of satellite FNR can be considered to be effective and make sense.
All these discussed above has been method in the revised manuscript, please refer to the Line 258-348.

Minor Comments:

1. Lines 116 to 120: Do you see similar seasonal cycle of HCHO from ground?

R: Thanks for the comment. As shown in Figure R1, the monthly averages of ground surface HCHO at 13:00-14:00 observed by LP-DOAS also show the similar seasonal cycle with satellite observation, that high in summer and low in winter. In addition, we have also calculated the averaged ground surface HCHO for the whole day, result also shows similar seasonal cycle (Figure R3). The seasonal ground surface HCHO concentrations is 2.25 ± 0.40 ppbv in spring, 3.08 ± 0.51 ppbv in summer, 2.47 ± 0.61 ppbv in autumn and 2.21 ± 0.88 ppbv in winter, respectively. We have added it in the revised manuscript, please refer to the Line 133-134. The division of seasons is referred to the response below. We have also added Figure R3 into Figure 1 of the revised manuscript to characterize the seasonal variation of ground surface HCHO.

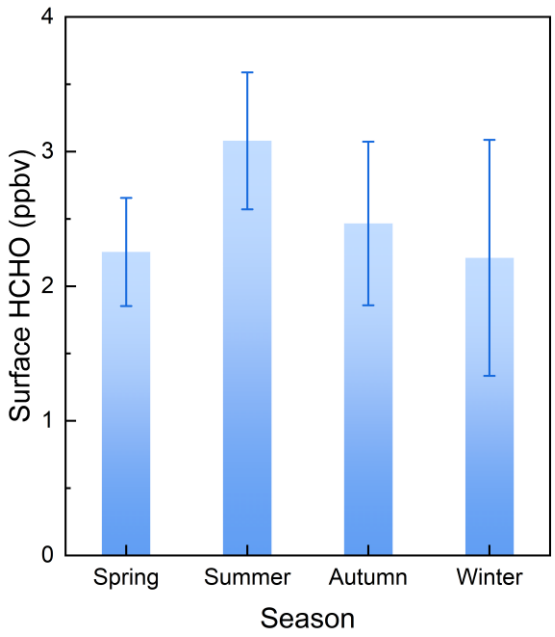

Figure R3. Seasonal averaged ground surface HCHO concentrations observed by LP-DOAS during 2018-2019.

2. Figure 1: Please define season here.

R: Thanks for the suggestion. In the study, seasons were divided as March, April, and May for spring, June, July, and August for summer, September, October, and November for autumn, December, January and February for winter. We have also defined seasons in the revised manuscript, please also refer to Line 120-122.

3. Figure 1: I'd suggest include error bars to indicate spatial variation.

R: Thanks for the suggestion. We have added error bars to Figure 1 to indicate the spatial variation. The seasonal variation of ground surface HCHO was also added as Figure 1(d). Please refer to the updated Figure 1 in the revised manuscript.

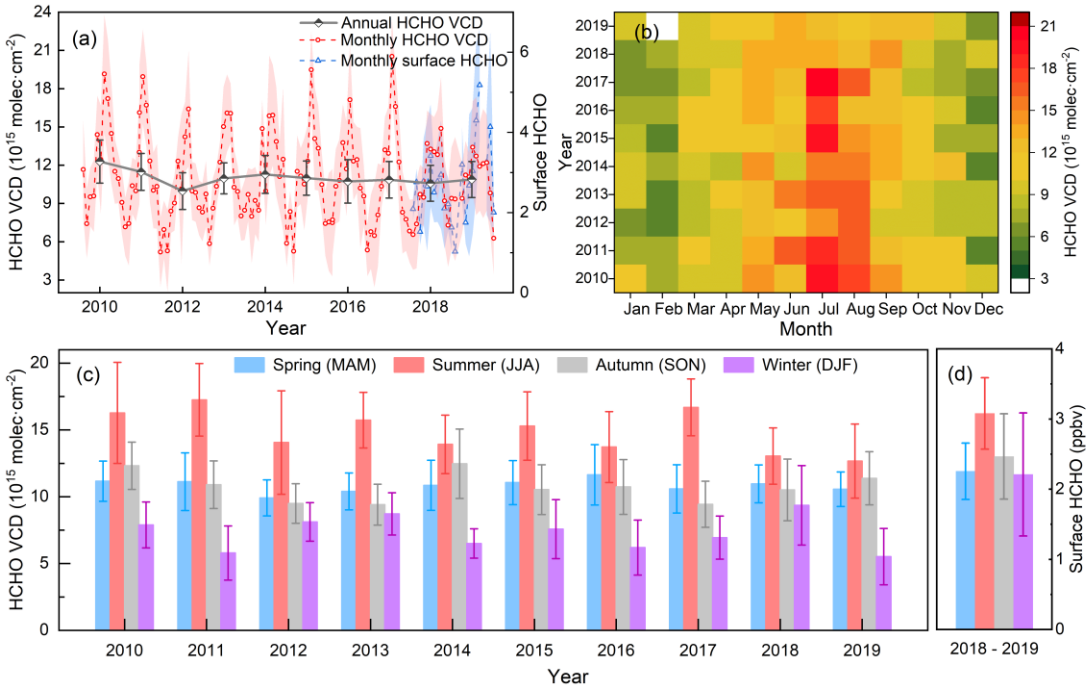

Figure R4. OMI and LP-DOAS observed time series of HCHO in Shanghai. (a) to (c) reflect the annual, monthly and seasonal variations of HCHO VCD during 2010-2019, error bars indicate the spatial variation of HCHO VCD. (d) reflects the monthly variation of surface HCHO observed by LP-DOAS during 2018-2019. (Figure 1 in the manuscript).

4. Figure 3: Why did you choose to show seasonal cycle only? I think it will be more interesting if you can show the time series from 2010 to 2018, and see how HCHO is correlated with each factor. This may also help explain the inter-annual variability of HCHO.

R: Thank you for the comments. We have followed the suggestion and analyzed the relationship between time series of HCHO VCDs and meteorological variables including temperature, sunshine hours, precipitation, and relative humidity via the linear regression. The stepwise regression results show that, the correlation between meteorological variables and HCHO VCD is not significant except temperature. Therefore, only the linear regression of temperature contribution and HCHO VCD was shown in Figure R4. We have presented Figure R4 in the manuscript as Figure 3, and moved the original Figure 3 to supplement and marked it as Figure S2.

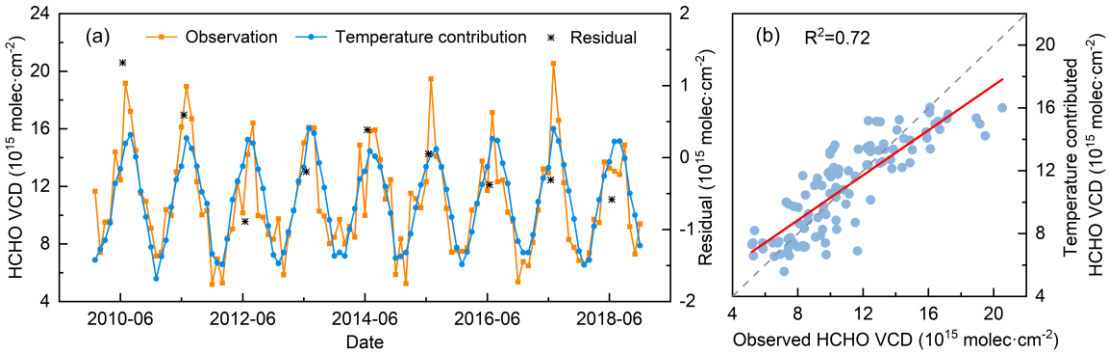

Figure R4. Monthly HCHO VCDs and the temperature contribution in Shanghai during 2010-2018. (a) reflects the temporal variations and (b) illustrates the correlation analysis. The black points represent the annual average residuals.

The temperature contribution was strongly correlated with the observed HCHO VCD ($R^2 = 0.72$), which means that temperature can explain about 72% of the variation of HCHO VCD. The remaining part that cannot be explained by temperature appears in the form of residual, which is considered as the influences of other changing factors such as anthropogenic emissions (Li et al., 2019). We have also noticed that the residual in summer in some years would be particularly large, which indicates that in addition to temperature, there are other factors affecting HCHO VCD significantly in summer.

Therefore, we have further analyzed the phenomenon in June that the HCHO VCD declines when the temperature rises, the precipitation and relative humidity rises significantly, as shown in Figure S2. Shanghai has a subtropical monsoon climate with rain and heat in the same period. Precipitation and relative humidity surged in June, while HCHO VCD decreased slightly with the increase of temperature. High relative humidity in July favoured the wet deposition of HCHO largely and offset the impact of rising temperature, resulting in a small decrease in HCHO VCDs.

We have regarded the changes of monthly averaged relative humidity and HCHO VCD as two variables, as shown in Eq. (R1) (R2).

$$\Delta RH_i = RH_i - RH_{i-1} \quad \text{(R1)}$$

$$\Delta VCD_i = VCD_i - VCD_{i-1} \quad \text{(R2)}$$

where ΔRH_i and ΔVCD_i are the changes of relative humidity and HCHO VCD for month i (Jun, Jul and Aug) between 2010 and 2018, respectively.

Then, the response of monthly HCHO VCDs variations to the changes of monthly relative humidity has been examined by Fisher's exact test (Clinton et al., 2020). We have defined the ΔVCD_i exceeding $\pm 1\times10^{15}$ molec·cm^{-2} (about 10% of VCD_{range}) as an obvious increase or decrease of HCHO VCDs. And two conditions of 10% and 20% changes on RH_{range} were checked. The RH_{range} and VCD_{range} is the range of relative humidity and HCHO VCDs between respective maximum and minimum, which are represented by the subscripts of 'max' and 'min' respectively, as expressed in Eq. (R3) and (R4).

$$RH_{range} = RH_{max} - RH_{min} \quad \text{(R3)}$$

$$VCD_{range} = VCD_{max} - VCD_{min} \quad \text{(R4)}$$

Results of Fisher's exact test determined that when ΔRH_i exceeds 10% of RH_{range}, no

significant correlation is found between these two variables (P = 0.637); when the change degree goes up to 20%, there is a significant correlation between them (P < 0.05). Therefore, it can be inferred that the variation in HCHO VCDs is related to the significant change of relative humidity in summer.
All these discussed above has been method in the revised manuscript, please refer to the Line 156-175.

5. Figure 4: Need to include secondary HCHO from both anthropogenic and biogenic VOCs.
R: As replied above, the secondary HCHO from anthropogenic and biogenic VOCs have been estimated. Considering the lack of continuous BVOCs emission data, we only have plotted the primary emission and secondary production from anthropogenic sources. The results are shown in Figure R5 (Figure 4 in the revised manuscript). The biogenic contribution of HCHO and its uncertainty were discussed in the manuscript, and result in 2014 was marked as red cross in Figure R5(b). Please refer to Line 182 for detailed.

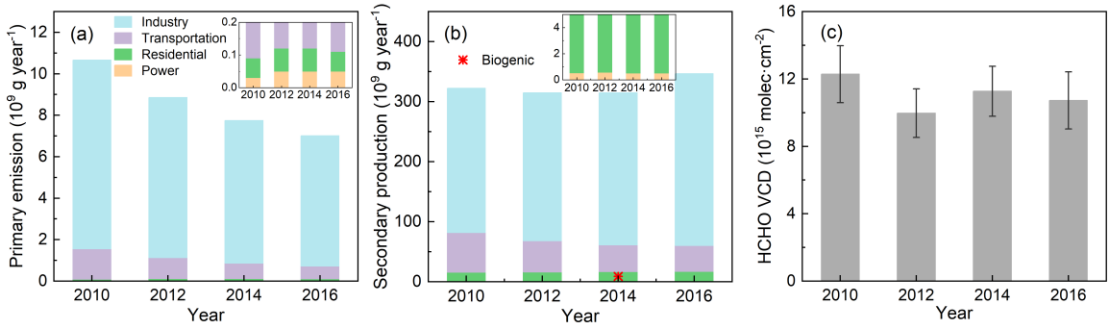

Figure R5. Primary emissions and estimated secondary productions of HCHO from anthropogenic NMVOCs, biogenic contribution of HCHO in 2014 was marked as red cross in Figure R5(b).

6. Figure 7: How do you define urban vs. rural areas?
R: Thanks for the comment. We have defined the urban and rural areas according to its distance from the city center of Shanghai (31.24 °N, 121.48 °E). The distances from Jiangwan campus of Fudan University and Dianshan Lake to the city center are about 12 km and 50 km, respectively. Considering the civilization and development of Shanghai whole city, it would be more accurate to use suburban area instead of rural area. Therefore, we have taken areas around Jiangwan campus of Fudan University, which is closer to the city center, as the representative of the urban, and areas around Dianshan Lake, which is much far from the city center, as the representative of the suburban. The distances away from city center were also supplemented in the manuscript. Please refer to Line 242-244.

7. Figure 8: It's unclear whether you're showing FNR and ozone for one site or three sites together? If one site, which site?
R: Thanks for the comments. Figure 8 showed the three cases only observed at the

Jiangwan campus of Fudan University. We have clarified it and please refer to Line 274-276.

Reference:

Chan, K. L., Wang, Z. R., Ding, A. J., Heue, K. P., Shen, Y. C., Wang, J., Zhang, F., Shi, Y. N., Hao, N., and Wenig, M.: MAX-DOAS measurements of tropospheric NO_2 and HCHO in Nanjing and a comparison to ozone monitoring instrument observations, Atmos Chem Phys, 19, 10051-10071, https://doi.org/10.5194/acp-19-10051-2019, 2019.

Clinton, S., Johnson, J., Lambirth, K., Sun, S., Brouwer, C., Keen, O., Redmond, M., Fodor, A., and Gibas, C.: Sediment Microbial Diversity in Urban Piedmont North Carolina Watersheds Receiving Wastewater Input, Water-Sui, 12, 16, https://doi.org/10.3390/w12061557, 2020.

Duncan, B. N., Yoshida, Y., Olson, J. R., Sillman, S., Martin, R. V., Lamsal, L., Hu, Y. T., Pickering, K. E., Retscher, C., Allen, D. J., and Crawford, J. H.: Application of OMI observations to a space-based indicator of NO_x and VOC controls on surface ozone formation, Atmos Environ, 44, 2213-2223, https://doi.org/10.1016/j.atmosenv.2010.03.010, 2010.

Fan, J. C., Ju, T. Z., Wang, Q. H., Gao, H. Y., Huang, R. R., and Duan, J. L.: Spatiotemporal variations and potential sources of tropospheric formaldehyde over eastern China based on OMI satellite data, Atmos Pollut Res, 12, 272-285, https://doi.org/10.1016/j.apr.2020.09.011, 2021.

Fioletov, V. E., McLinden, C. A., Krotkov, N., Moran, M. D., and Yang, K.: Estimation of SO2 emissions using OMI retrievals, Geophys Res Lett, 38, 5, https://doi.org/10.1029/2011gl049402, 2011.

Gao, W., Tie, X. X., Xu, J. M., Huang, R. J., Mao, X. Q., Zhou, G. Q., and Chang, L. Y.: Long-term trend of O-3 in a mega City (Shanghai), China: Characteristics, causes, and interactions with precursors, Sci Total Environ, 603, 425-433, https://doi.org/10.1016/j.scitotenv.2017.06.099, 2017.

Jin, X. M., Fiore, A., Boersma, K. F., De Smedt, I., and Valin, L.: Inferring Changes in Summertime Surface Ozone-NO_x-VOC Chemistry over US Urban Areas from Two Decades of Satellite and Ground-Based Observations, Environ Sci Technol, 54, 6518-6529, https://doi.org/10.1021/acs.est.9b07785, 2020.

Li, K., Jacob, D. J., Liao, H., Shen, L., Zhang, Q., and Bates, K. H.: Anthropogenic drivers of 2013-2017 trends in summer surface ozone in China, P Natl Acad Sci USA, 116, 422-427, https://doi.org/10.1073/pnas.1812168116, 2019.

Liu, Y., Li, L., An, J., Zhang, W., Yan, R., Huang, L., Huang, C., Wang, H., Wang, Q., and Wang, M.: Emissions, Chemical Composition, and Spatial and Temporal Allocation of the BVOCs in the Yangtze River Delta Region in 2014, ENVIRONMENTAL SCIENCE, 39, 608-617, 2018a.

Liu, Y., Li, L., An, J. Y., Huang, L., Yan, R. S., Huang, C., Wang, H. L., Wang, Q., Wang, M., and Zhang, W.: Estimation of biogenic VOC emissions and its impact on ozone formation over the Yangtze River Delta region, China, Atmos Environ, 186, 113-128, https://doi.org/10.1016/j.atmosenv.2018.05.027, 2018b.

Luo, H. H., Yang, L. F., Yuan, Z. B., Zhao, K. H., Zhang, S., Duan, Y. S., Huang, R. Z., and Fu, Q. Y.: Synoptic condition-driven summertime ozone formation regime in Shanghai and the implication for dynamic ozone control strategies, Sci Total Environ, 745, 12, https://doi.org/10.1016/j.scitotenv.2020.141130, 2020.

Marais, E. A., Jacob, D. J., Kurosu, T. P., Chance, K., Murphy, J. G., Reeves, C., Mills, G., Casadio, S.,

Millet, D. B., Barkley, M. P., Paulot, F., and Mao, J.: Isoprene emissions in Africa inferred from OMI observations of formaldehyde columns, Atmos Chem Phys, 12, 6219-6235, https://doi.org/10.5194/acp-12-6219-2012, 2012.
McLinden, C. A., Fioletov, V., Boersma, K. F., Krotkov, N., Sioris, C. E., Veefkind, J. P., and Yang, K.: Air quality over the Canadian oil sands: A first assessment using satellite observations, Geophys Res Lett, 39, 8, https://doi.org/10.1029/2011gl050273, 2012.
Miller, C. C., Jacob, D. J., Marais, E. A., Yu, K. R., Travis, K. R., Kim, P. S., Fisher, J. A., Zhu, L., Wolfe, G. M., Hanisco, T. F., Keutsch, F. N., Kaiser, J., Min, K. E., Brown, S. S., Washenfelder, R. A., Abad, G. G., and Chance, K.: Glyoxal yield from isoprene oxidation and relation to formaldehyde: chemical mechanism, constraints from SENEX aircraft observations, and interpretation of OMI satellite data, Atmos Chem Phys, 17, 8725-8738, https://doi.org/10.5194/acp-17-8725-2017, 2017.
Palmer, P. I., Abbot, D. S., Fu, T. M., Jacob, D. J., Chance, K., Kurosu, T. P., Guenther, A., Wiedinmyer, C., Stanton, J. C., Pilling, M. J., Pressley, S. N., Lamb, B., and Sumner, A. L.: Quantifying the seasonal and interannual variability of North American isoprene emissions using satellite observations of the formaldehyde column, J. Geophys. Res.-Atmos., 111, 14, https://doi.org/10.1029/2005jd006689, 2006.
Schroeder, J. R., Crawford, J. H., Fried, A., Walega, J., Weinheimer, A., Wisthaler, A., Muller, M., Mikoviny, T., Chen, G., Shook, M., Blake, D. R., and Tonnesen, G. S.: New insights into the column CH_2O/NO_2 ratio as an indicator of near-surface ozone sensitivity, J. Geophys. Res.-Atmos., 122, 8885-8907, https://doi.org/10.1002/2017jd026781, 2017.
Shen, L., Jacob, D. J., Zhu, L., Zhang, Q., Zheng, B., Sulprizio, M. P., Li, K., De Smedt, I., Abad, G. G., Cao, H. S., Fu, T. M., and Liao, H.: The 2005-2016 Trends of Formaldehyde Columns Over China Observed by Satellites: Increasing Anthropogenic Emissions of Volatile Organic Compounds and Decreasing Agricultural Fire Emissions, Geophys Res Lett, 46, 4468-4475, https://doi.org/10.1029/2019gl082172, 2019.
Song, Y., Zhang, Y., Wang, Q., and An, J.: Estimation of biogenic VOCs emissions in Eastern China based on remote sensing data, Acta Sci Circum, 32, 2216-2227, 2012.
Souri, A. H., Nowlan, C. R., Wolfe, G. M., Lamsal, L. N., Miller, C. E. C., Abad, G. G., Janz, S. J., Fried, A., Blake, D. R., Weinheimer, A. J., Diskin, G. S., Liu, X., and Chance, K.: Revisiting the effectiveness of HCHO/NO2 ratios for inferring ozone sensitivity to its precursors using high resolution airborne remote sensing observations in a high ozone episode during the KORUS-AQ campaign, Atmos Environ, 224, https://doi.org/ARTN 117341
10.1016/j.atmosenv.2020.117341, 2020.
Wang, H., Wu, Q. Z., Guenther, A. B., Yang, X. C., Wang, L. N., Xiao, T., Li, J., Feng, J. M., Xu, Q., and Cheng, H. Q.: A long-term estimation of biogenic volatile organic compound (BVOC) emission in China from 2001-2016: the roles of land cover change and climate variability, Atmos Chem Phys, 21, 4825-4848, https://doi.org/10.5194/acp-21-4825-2021, 2021a.
Wang, Y. J., Tan, X. J., Huang, L., Wang, Q., Li, H. L., Zhang, H. Y., Zhang, K., Liu, Z. Y., Traore, D., Yaluk, E., Fu, J. S., and Li, L.: The impact of biogenic emissions on ozone formation in the Yangtze River Delta region based on MEGANv3.1, Air Qual. Atmos. Health, 14, 763-774, https://doi.org/10.1007/s11869-021-00977-0, 2021b.
Wang, Y. P., Wang, Z. F., Yu, C., Zhu, S. Y., Cheng, L. X., Zhang, Y., and Chen, L. F.: Validation of OMI HCHO Products Using MAX-DOAS observations from 2010 to 2016 in Xianghe, Beijing: Investigation of the Effects of Aerosols on Satellite Products, Remote Sens-Basel, 11, 21, https://doi.org/10.3390/rs11020203, 2019.

Xue, R. B., Wang, S. S., Li, D. R., Zou, Z., Chan, K. L., Valks, P., Saiz-Lopez, A., and Zhou, B.: Spatio-temporal variations in NO_2 and SO_2 over Shanghai and Chongming Eco-Island measured by Ozone Monitoring Instrument (OMI) during 2008-2017, J Clean Prod, 258, 14, https://doi.org/10.1016/j.jclepro.2020.120563, 2020.

Zhu, L., Jacob, D. J., Mickley, L. J., Marais, E. A., Cohan, D. S., Yoshida, Y., Duncan, B. N., Abad, G. G., and Chance, K. V.: Anthropogenic emissions of highly reactive volatile organic compounds in eastern Texas inferred from oversampling of satellite (OMI) measurements of HCHO columns, Environ Res Lett, 9, 7, https://doi.org/10.1088/1748-9326/9/11/114004, 2014.

Zhu, L., Mickley, L. J., Jacob, D. J., Marais, E. A., Sheng, J. X., Hu, L., Abad, G. G., and Chance, K.: Long-term (2005-2014) trends in formaldehyde (HCHO) columns across North America as seen by the OMI satellite instrument: Evidence of changing emissions of volatile organic compounds, Geophys Res Lett, 44, 7079-7086, https://doi.org/10.1002/2017gl073859, 2017.

Response to review #2

We thank the reviewer for the constructive comments and suggestions, which are very positive to improve scientific content of the manuscript. We have revised the manuscript appropriately and addressed all the reviewer's comments point-by-point for consideration as below. The remarks from the reviewer are shown in black, and our responses are shown in blue color. All the page and line numbers mentioned following are refer to the revised manuscript without change tracked.

This study examined long-term HCHO columns in Shanghai with OMI and ground-based remote sensing observations. The author also studied the ozone sensitivity in Shanghai and proposed a correction factor to satellite HCHO to NO2 ratio. The authors found that applying such a correction results in ozone formation is more likely to be under the VOC-limited regime. In my view, this work is among few studies exclusively focusing on HCHO observations and ozone sensitivity in China, thus is appropriate for publication at ACP subject to the following concerns.

1. The authors examined monthly averaged columns at a spatial resolution of 0.01°×0.01° degree. I am not sure whether there would be enough pixels in each grid cell to reduce the uncertainty in mean HCHO column to a much lower and acceptable level. This could be a potential issue in the winter seasons when SZA is high and the light path is long.

R: Thanks for your professional comments. In order to check whether there were enough pixels in each grid, we have counted the number of days that each grid has been assigned with HCHO VCDs between 2010 and 2019 on monthly scale. Here, we have defined the effective observation days (EODs) as the number of days that once any grid within Shanghai areas has been still designated after the data quality filtering. Afterwards, we have calculated the percentages of areas with observed days reached 60% EODs for every month during 2010-2019, results are shown in Table R1. For example, in January, about 80% areas of Shanghai have been assigned with HCHO VCDs during more than 60% of the total EODs.

Table R1. Proportion of areas with observed days reached 60% EODs in each month of 2010-2019.

Month	Proportion	Month	Proportion
January	79.9% ± 24.6%	July	72.2% ± 31.8%
February	61.6% ± 33.6%	August	69.7% ± 25.7%
March	87.7% ± 16.5%	September	71.2% ± 33.4%
April	94.3% ± 9.1%	October	59.7% ± 30.9%
May	86.1% ± 30.2%	November	88.5% ± 13.3%
June	33.4% ± 25.1%	December	84.4% ± 18.6%

Table R1 reveals that the winter months did not show the obvious low proportion, while

the proportion in June is much lower. It can be explained by the impacts of abundant precipitation in June (as shown in Figure S2), which leads to only a small amount of areas were assigned with HCHO VCD on the EOD after screening by cloud fraction. So, we considered that the monthly averaged HCHO VCDs can be the representative of the mean level of HCHO in Shanghai when the temporal patterns were discussed in the manuscript. While the spatial characteristics have been investigated with high spatial resolution only when more EODs have been oversampled, e.g. in seasonal with multiple years averaged.

2. Did the authors correct the well-known drift in OMI SAO HCHO product? If not, please do so and update the results accordingly.

R: Thanks for your suggestions. Previous studies mentioned that OMI-SAO HCHO columns display significant drift due to instrument aging (Marais et al., 2012; Zhu et al., 2014; Zhu et al., 2017), in which OMI HCHO Version 2.0 data were used. However, the updated product (OMI HCHO Version 3.0) were used in this study, which has a significant improvement in treating the increasing trend of background values (https://aura.gesdisc.eosdis.nasa.gov/data/Aura_OMI_Level2/OMHCHO.003/doc/README.OMHCHO.pdf).

In order to check whether there is still obvious drift, we have performed temporal linear regression of the deseasonalized monthly averaged HCHO columns during 2010-2019 for remote pacific region (29°-33°N, 160°-140°W) around the same latitude as Shanghai (Zhu et al., 2017). Zonal mean HCHO columns have been calculated with 0.5° latitude steps. It was found that there was no obvious linear trend for the deseasonalized HCHO VCDs on monthly scale in those eight zonal latitude ranges (R^2 ranged from 0.06 to 0.19 with average of 0.11), suggesting that the updated OMI HCHO product used in this study does not include the obvious drift. Figure R2 shows the time series of deseasonalized zonal mean HCHO VCDs for the highest and lowest latitudes on monthly scale. We have clarified in the manuscript, please refer to Line 99-101.

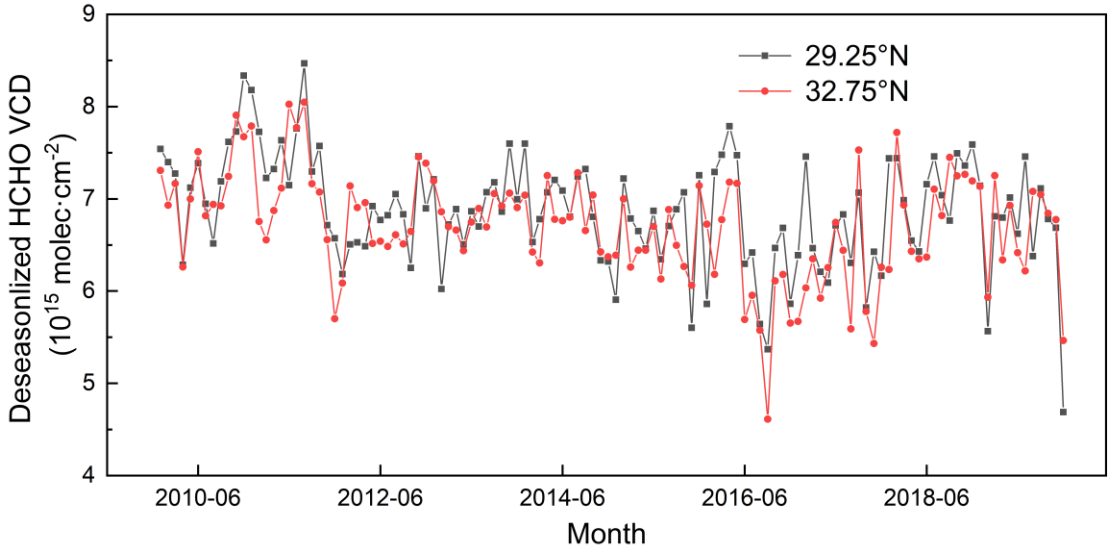

Figure R2. The time series of deseasonalized zonal monthly mean HCHO VCDs of different latitudes in the remote pacific region (29°-33°N, 160°-140°W). Monthly variations of zonal mean

HCHO VCD with the maximum and minimum latitude are exhibited as the example (29.25°N and 32.75°N stands for range of 29.0°-29.5°N and 32.5°-33.0°N, respectively).

3. In page 7, please clarify how to get the HCHO emission rate? Is HCHO mainly secondary? If so, how to determine HCHO yields from NMVOCs? The authors may also want to consider the lower HCHO yields from NMVOCs as NOx emissions drop in the study period.

R: Thank you for the professional comments. Figure 7 in the original manuscript reflects the annual anthropogenic HCHO primary emissions and does not include the secondary production of HCHO. However, secondary production of HCHO from anthropogenic and biogenic sources has contributed greatly to HCHO (Zhu et al., 2017; Shen et al., 2019). As suggested by Reviewer #1, we have also considered the secondary production of HCHO in the revised manuscript, including anthropogenic and biogenic sources. Please refer to Line 176-205.

In order to get the secondary production of HCHO from anthropogenic sources, Non-methane volatile organic compounds (NMVOCs) emission inventory based on the SAPRC07 mechanism species from Multi-resolution Emission Inventory for China (MEIC) was used for years of 2010, 2012, 2014 and 2016. Secondary production of HCHO has been calculated based on 1-day HCHO yields of several NMVOCs under high-NO_x condition (Shen et al., 2019). Table R2 summarizes the primary emissions and secondary productions of HCHO from different sectors of anthropogenic sources.

Table R2. The primary emissions and estimated secondary productions of HCHO in Shanghai from anthropogenic NMVOCs based on SAPRC07 mechanism species.

Year		Estimated HCHO production from each sector (10^9 g)				
		Industry	Power	Residential	Transportation	Total
2010	Primary[1]	9.10	0.03	0.06	1.47	10.66
	Secondary[2]	240.58	0.52	15.14	66.04	322.28
2012	Primary	7.73	0.05	0.07	1.01	8.86
	Secondary	246.67	0.57	15.67	51.91	314.82
2014	Primary	6.88	0.05	0.07	0.74	7.74
	Secondary	253.32	0.50	16.44	44.32	314.58
2016	Primary	6.29	0.05	0.06	0.61	7.01
	Secondary	286.36	0.51	16.64	43.14	346.65

[1] Primary indicates HCHO that is directly emitted by anthropogenic sources from MEIC inventory.

[2] Secondary indicates HCHO that is produced by anthropogenic NMVOCs, which is calculated based on 1-day HCHO yields.

Regardless of the primary emissions or secondary productions of HCHO, industry sector corresponds to the largest yield, followed by transportation, residential, and the power. For the temporal trend, the primary emission of HCHO keeps decreasing (about 34.2% compared to 2010), while secondary produced HCHO did not change

significantly. The increase of secondary HCHO yields in 2016 was mainly due to the increased production from industry sector. In addition, the changes and proportional relationships between primary emission and secondary production of HCHO for different sectors are different, which suggests the VOCs source profiles of different sectors would affect the amount of secondary HCHO production.

HCHO yield from biogenic sources can be estimated from BVOCs emission inventory. Model of Emissions of Gases and Aerosols from Nature (MEGAN) is widely used to simulate the emission of BVOCs. As we currently cannot use MEGAN to accurately simulate four-year (2010, 2012, 2014, 2016) BVOCs emissions, we have used the annual total BVOCs emissions of Shanghai in 2014 (about 1.2×10^4 t) for the estimation (Liu et al., 2018a; Liu et al., 2018b). Isoprene, methanol and monoterpenes were dominant compositions of BVOCs and accounted about 81.3% of the total. We have calculated HCHO yields contributed by isoprene, methanol and monoterpenes, as shown in Table R3.

Table R3. The annual BVOCs emissions and HCHO yields over Shanghai in 2014.

BVOC	Emission (10^9 g)	HCHO yield (10^9 g)
Isoprene	4.63	4.70
Methanol	4.26	3.99
Monoterpenes	0.86	0.38
Total	9.75	9.07

Accordingly, HCHO yield from BVOCs emission was estimated to be about 9.07×10^9 g, and mostly produced from isoprene and methanol. The calculated HCHO yield from BVOCs emission is similar to that of previous study during 2005-2016 (Shen et al., 2019). In addition, compared with anthropogenic sources, HCHO yield from BVOCs is much smaller, which indicates that the anthropogenic is the main contributor of secondary production of HCHO in Shanghai (Shen et al., 2019; Fan et al., 2021).

As shown in Table R4, we have also reviewed the related studies about the BVOCs emissions in Shanghai and its surrounding areas (the Yangtze River Delta) in relevant years. Wang et al. (2021a) assessed the impacts of land cover change and climate variability on BVOCs emissions in China from 2001 to 2016, in which variations of BVOCs emissions in Shanghai over the years were extremely small. Considering the different input dataset and settings would bring large differences in the simulated results, it was unfeasible to use BVOCs emissions from different studies for the investigation of temporal variation. Therefore, the BVOCs emissions in 2014 were used to basically characterize the approximate level of BVOCs from 2010 to 2016 in this study.

Table R4. Comparison of simulated BVOCs emissions in Shanghai (SH) and the Yangtze River Delta (YRD) based on MEGAN.

Simulated year	Reference	MEGAN version	Region	BVOCs emission (10^4 t)
2010	Song et al. (2012)[1]	V 2.04	YRD	110
			SH	0.122
2014	Liu et al. (2018a; 2018b)[2]	V 2.10	YRD	188.6
			SH	1.2
2016	Wang et al. (2021b)[3]	V 3.1	YRD	162 [1]
			SH	~ 0.34 [4]

[1] Total annual emission inferred from the simulated BVOCs emissions in January, April, July and October.

[2] A variety of methods were used to reduce the uncertainty of plant functional types (PFT) database. The proportions of dominant components of BVOCs were also provided.

[3] BVOCs emission was simulated without drought stress.

[4] It is BVOCs emissions in July, which has been inferred from Fig. S3 of Wang et al. (2021b).

In addition, it should be noted that HCHO yield was also impacted by the NO_x levels, e.g. RO_2 radical from VOCs react with HO_2 to from organic peroxides under low NO_x condition. This process reduces the reaction of RO_2 and NO, which in turn decreases the production of HCHO, therefore, HCHO yield from VOCs is proportional to NO_x condition (Palmer et al., 2006; Marais et al., 2012; Miller et al., 2017). In this study, the estimation using a fixed HCHO yield may overestimate HCHO production in later years due to the decreases of NO_x in Shanghai (Xue et al., 2020). In previous studies, the proportional relationship between HCHO yield and NO_x condition was usually obtained when 1 ppbv of NO_x regard as the high condition, and 0.1 ppbv of NO_x regard as low condition (Palmer et al., 2006; Marais et al., 2012; Miller et al., 2017). However, the NO_x concentration in Shanghai is still relatively higher (basically 30-60 ppbv in urban) (Gao et al., 2017). Therefore, in such a high NO_x condition, the effect of NO_x decreases on HCHO yield needs to be further studied.

Minor comments:

1. Page 2, line 39-40, please include GOME-2 A, B, and C

R: Thanks for the suggestion. We have added GOME-2 A, B, and C in the Introduction, please refer to Line 39.

2. Page 3, line 76, please change “in a day” to “in the daytime”

R: We have corrected ‘in a day’ to ‘in the daytime’. Please refer to Line 76.

3. Page 3, line 80, please change “pixels” to “rows”

R: We have corrected ‘pixels’ to ‘rows’. Please refer to Line 80.

4. Page 3, line 81, here and elsewhere, please change “~” to “-”. “~” means “approximately”

R: Thanks for the reminding. We have changed ‘~’ to ‘-’. Please refer to Line 81.

5. Page 3, line 92-93, I think by using MainQualityFlag=0 as the criterion, you have filtered out pixels affected by row anomalies already.

R: Thanks for your comments. Pixels flagged with 0 in field MainDataQualityFlag were considered to be passed quality check. However, in OMHCHO V3.0 product, field XtrackQualityFlags has been carried over from the L1b product to characterize pixels affected by the row anomaly. We have tested and found that the usage of XtrackQualityFlags during the filtering process can affect the results. As shown in Figure R3, under the two filtering conditions, HCHO VCDs have obvious differences in some regions. In addition, Figure R3(a) exists a track with abnormally high value, which basically disappeared after being filtered by using XtrackQualityFlags. It means that including XtrackQualityFlags in filtering criterion in addition to MainDataQualityFlag would be effective.

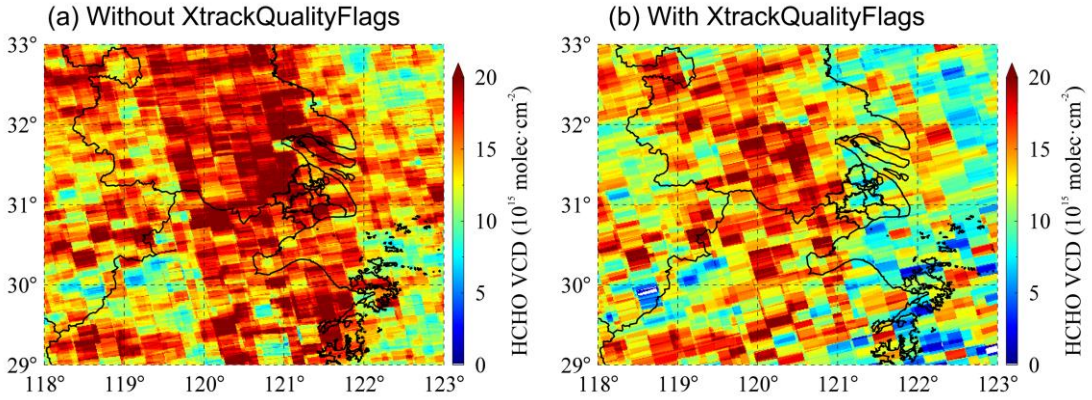

Figure R3. Spatial distribution of HCHO VCDs of Shanghai and surrounding areas in October 2010 under different filter conditions of (a) without XtrackQualityFlags and (b) with XtrackQualityFlags.

6. Page 5, line 127-129, could you please explain the spatial variations in HCHO columns. Is the spatial pattern consistent with emissions?

R: Thanks for your comments. For determining whether the spatial variations in HCHO VCD is consistent with local emissions, we have displayed the spatial distribution of anthropogenic NMVOCs in Shanghai in 2017 with high resolution of 4 km×4 km in Figure R4 (An et al., 2021). It can be seen that the hotspots of NMVOCs emission were concentrated in the city center, while the highest HCHO VCD appeared in the relatively remote Qingpu district, where the NMVOCs emissions were relatively low. Obviously, the anthropogenic emissions and HCHO VCD do not coincide well in the spatial pattern, and the high value of HCHO VCD in Qingpu district cannot be directly explained by the emission of anthropogenic NMVOCs.

Not only high HCHO VCD observed by satellites, but also high concentrations of surface HCHO have been measured in Qingpu District (e.g. Su et al., 2019; Zhang et al., 2021). Impact of air masses transport containing high concentrations of reactive VOCs from adjacent Zhejiang Province and Jiangsu Province was reported (Zhang et al., 2020). As shown in Figure R4, the anthropogenic NMVOCs inventory in the Yangtze River Delta also displays that there were obvious sources of NMVOCs in the

southern part of Jiangsu and the northern part of Zhejiang. The high local atmospheric oxidation capacity leads to the rapid degradation of VOCs, which in turn enhances the contributions of anthropogenic NMVOCs to the local HCHO production in Qingpu district (Zhang et al., 2021).

In addition, model simulation showed that isoprene plays an important role in the production of HCHO as the precursor, and it can contribute about 36% of the production of HCHO during O_3 formation episodes from April to June in 2018 in Qingpu district (Zhang et al., 2021). The abundant BVOCs in Qingpu district may be another important reason for the high HCHO VCD. Please refer to Line 139-143.

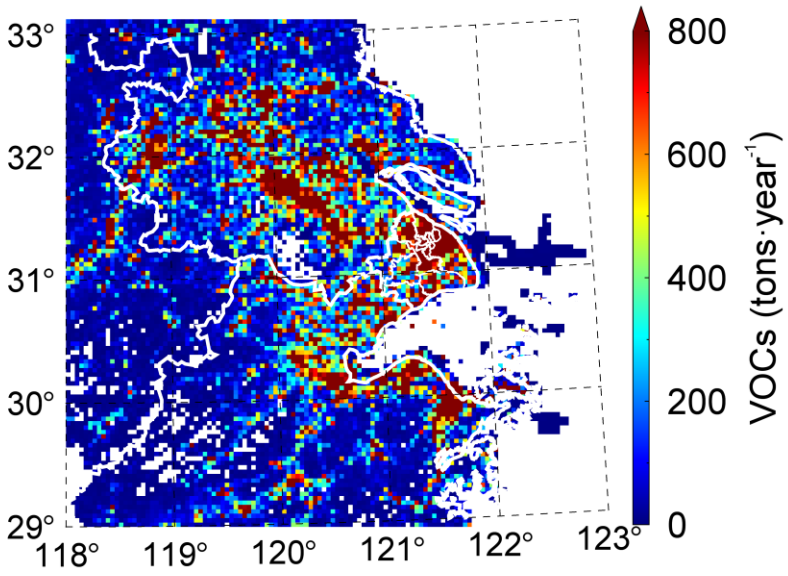

Figure R4. Anthropogenic NMVOCs emissions in Shanghai in 2017. The inventory data is available from An et al. (2021).

Reference:

An, J. Y., Huang, Y. W., Huang, C., Wang, X., Yan, R. S., Wang, Q., Wang, H. L., Jing, S. A., Zhang, Y., Liu, Y. M., Chen, Y., Xu, C., Qiao, L. P., Zhou, M., Zhu, S. H., Hu, Q. Y., Lu, J., and Chen, C. H.: Emission inventory of air pollutants and chemical speciation for specific anthropogenic sources based on local measurements in the Yangtze River Delta region, China, Atmos Chem Phys, 21, 2003-2025, https://doi.org/10.5194/acp-21-2003-2021, 2021.

Fan, J. C., Ju, T. Z., Wang, Q. H., Gao, H. Y., Huang, R. R., and Duan, J. L.: Spatiotemporal variations and potential sources of tropospheric formaldehyde over eastern China based on OMI satellite data, Atmos Pollut Res, 12, 272-285, https://doi.org/10.1016/j.apr.2020.09.011, 2021.

Gao, W., Tie, X. X., Xu, J. M., Huang, R. J., Mao, X. Q., Zhou, G. Q., and Chang, L. Y.: Long-term trend of O-3 in a mega City (Shanghai), China: Characteristics, causes, and interactions with precursors, Sci Total Environ, 603, 425-433, https://doi.org/10.1016/j.scitotenv.2017.06.099, 2017.

Liu, Y., Li, L., An, J., Zhang, W., Yan, R., Huang, L., Huang, C., Wang, H., Wang, Q., and Wang, M.:

Emissions, Chemical Composition, and Spatial and Temporal Allocation of the BVOCs in the Yangtze River Delta Region in 2014, ENVIRONMENTAL SCIENCE, 39, 608-617, 2018a.

Liu, Y., Li, L., An, J. Y., Huang, L., Yan, R. S., Huang, C., Wang, H. L., Wang, Q., Wang, M., and Zhang, W.: Estimation of biogenic VOC emissions and its impact on ozone formation over the Yangtze River Delta region, China, Atmos Environ, 186, 113-128, https://doi.org/10.1016/j.atmosenv.2018.05.027, 2018b.

Marais, E. A., Jacob, D. J., Kurosu, T. P., Chance, K., Murphy, J. G., Reeves, C., Mills, G., Casadio, S., Millet, D. B., Barkley, M. P., Paulot, F., and Mao, J.: Isoprene emissions in Africa inferred from OMI observations of formaldehyde columns, Atmos Chem Phys, 12, 6219-6235, https://doi.org/10.5194/acp-12-6219-2012, 2012.

Miller, C. C., Jacob, D. J., Marais, E. A., Yu, K. R., Travis, K. R., Kim, P. S., Fisher, J. A., Zhu, L., Wolfe, G. M., Hanisco, T. F., Keutsch, F. N., Kaiser, J., Min, K. E., Brown, S. S., Washenfelder, R. A., Abad, G. G., and Chance, K.: Glyoxal yield from isoprene oxidation and relation to formaldehyde: chemical mechanism, constraints from SENEX aircraft observations, and interpretation of OMI satellite data, Atmos Chem Phys, 17, 8725-8738, https://doi.org/10.5194/acp-17-8725-2017, 2017.

Palmer, P. I., Abbot, D. S., Fu, T. M., Jacob, D. J., Chance, K., Kurosu, T. P., Guenther, A., Wiedinmyer, C., Stanton, J. C., Pilling, M. J., Pressley, S. N., Lamb, B., and Sumner, A. L.: Quantifying the seasonal and interannual variability of North American isoprene emissions using satellite observations of the formaldehyde column, J. Geophys. Res.-Atmos., 111, 14, https://doi.org/10.1029/2005jd006689, 2006.

Shen, L., Jacob, D. J., Zhu, L., Zhang, Q., Zheng, B., Sulprizio, M. P., Li, K., De Smedt, I., Abad, G. G., Cao, H. S., Fu, T. M., and Liao, H.: The 2005-2016 Trends of Formaldehyde Columns Over China Observed by Satellites: Increasing Anthropogenic Emissions of Volatile Organic Compounds and Decreasing Agricultural Fire Emissions, Geophys Res Lett, 46, 4468-4475, https://doi.org/10.1029/2019gl082172, 2019.

Song, Y., Zhang, Y., Wang, Q., and An, J.: Estimation of biogenic VOCs emissions in Eastern China based on remote sensing data, Acta Sci Circum, 32, 2216-2227, 2012.

Su, W. J., Liu, C., Hu, Q. H., Zhao, S. H., Sun, Y. W., Wang, W., Zhu, Y. Z., Liu, J. G., and Kim, J.: Primary and secondary sources of ambient formaldehyde in the Yangtze River Delta based on Ozone Mapping and Profiler Suite (OMPS) observations, Atmos Chem Phys, 19, 6717-6736, https://doi.org/10.5194/acp-19-6717-2019, 2019.

Wang, H., Wu, Q. Z., Guenther, A. B., Yang, X. C., Wang, L. N., Xiao, T., Li, J., Feng, J. M., Xu, Q., and Cheng, H. Q.: A long-term estimation of biogenic volatile organic compound (BVOC) emission in China from 2001-2016: the roles of land cover change and climate variability, Atmos Chem Phys, 21, 4825-4848, https://doi.org/10.5194/acp-21-4825-2021, 2021a.

Wang, Y. J., Tan, X. J., Huang, L., Wang, Q., Li, H. L., Zhang, H. Y., Zhang, K., Liu, Z. Y., Traore, D., Yaluk, E., Fu, J. S., and Li, L.: The impact of biogenic emissions on ozone formation in the Yangtze River Delta region based on MEGANv3.1, Air Qual. Atmos. Health, 14, 763-774, https://doi.org/10.1007/s11869-021-00977-0, 2021b.

Xue, R. B., Wang, S. S., Li, D. R., Zou, Z., Chan, K. L., Valks, P., Saiz-Lopez, A., and Zhou, B.: Spatio-temporal variations in NO_2 and SO_2 over Shanghai and Chongming Eco-Island measured by Ozone Monitoring Instrument (OMI) during 2008-2017, J Clean Prod, 258, 14, https://doi.org/10.1016/j.jclepro.2020.120563, 2020.

Zhang, K., Li, L., Huang, L., Wang, Y. J., Huo, J. T., Duan, Y. S., Wang, Y. H., and Fu, Q. Y.: The impact of volatile organic compounds on ozone formation in the suburban area of Shanghai, Atmos Environ,

232, 11, https://doi.org/10.1016/j.atmosenv.2020.117511, 2020.
Zhang, K., Huang, L., Li, Q., Huo, J. T., Duan, Y. S., Wang, Y. H., Yaluk, E., Wang, Y. J., Fu, Q. Y., and Li, L.: Explicit modeling of isoprene chemical processing in polluted air masses in suburban areas of the Yangtze River Delta region: radical cycling and formation of ozone and formaldehyde, Atmos Chem Phys, 21, 5905-5917, https://doi.org/10.5194/acp-21-5905-2021, 2021.
Zhu, L., Jacob, D. J., Mickley, L. J., Marais, E. A., Cohan, D. S., Yoshida, Y., Duncan, B. N., Abad, G. G., and Chance, K. V.: Anthropogenic emissions of highly reactive volatile organic compounds in eastern Texas inferred from oversampling of satellite (OMI) measurements of HCHO columns, Environ Res Lett, 9, 7, https://doi.org/10.1088/1748-9326/9/11/114004, 2014.
Zhu, L., Mickley, L. J., Jacob, D. J., Marais, E. A., Sheng, J. X., Hu, L., Abad, G. G., and Chance, K.: Long-term (2005-2014) trends in formaldehyde (HCHO) columns across North America as seen by the OMI satellite instrument: Evidence of changing emissions of volatile organic compounds, Geophys Res Lett, 44, 7079-7086, https://doi.org/10.1002/2017gl073859, 2017.

OMI-observed HCHO in Shanghai, China during 2010-2019 and ozone sensitivity inferred by improved HCHO/NO_2 ratio

Danran Li [1], Shanshan Wang [1,2], Ruibin Xue [1], Jian Zhu [1], Sanbao Zhang[1], Zhibin Sun[1], and Bin Zhou [1,2,3]

[1]Shanghai Key Laboratory of Atmospheric Particle Pollution and Prevention (LAP[3]), Department of Environmental Science and Engineering, Fudan University, Shanghai, China
[2]Institute of Eco-Chongming (IEC), No. 20 Cuiniao Road, Shanghai 202162, China
[3]Institute of Atmospheric Sciences, Fudan University, Shanghai, 200433, China

Correspondence to: Shanshan Wang (shanshanwang@fudan.edu.cn)

Abstract. In recent years, satellite remote sensing has been increasingly used in the long-term observation of ozone (O_3) precursors and its formation regime. In this work, formaldehyde (HCHO) data from Ozone Monitoring Instrument (OMI) were used to analyse the temporal and spatial distribution of HCHO vertical column densities (VCDs) in Shanghai from 2010 to 2019. HCHO VCDs exhibited the highest value in summer and the lowest in winter, the high-VCD concentrated in western Shanghai. Temperature largely influence HCHO by affecting the biogenic emissions and photochemical reactions, and industry was the major anthropogenic source. The satellite observed formaldehyde to nitrogen dioxide ratio (FNR_{SAT}) reflects that the O_3 formation regime had significant seasonal characteristics and gradually manifested as transitional ozone formation regime dominated in Shanghai. The uneven distribution in space was mainly reflected as the higher FNR_{SAT} and surface O_3 concentration in ~~rural~~suburban area. To compensate the shortcoming of FNR_{SAT} that it can only characterize O_3 formation around satellite overpass time, correction of FNR_{SAT} was implemented with hourly surface FNR and O_3 data. After correction, O_3 formation regime showed the trend moving towards VOC-limited in both time and space, and regime indicated by FNR_{SAT} can better reflect O_3 formation for a day. This study can help us better understand HCHO characteristics and O_3 formation regime in Shanghai, and also provide a method to improve FNR_{SAT} for characterizing O_3 formation in a day, which will be significant for developing O_3 prevention and control strategies.

1 Introduction

Formaldehyde (HCHO) is an important trace gas in atmosphere. It has the irritating effect on human eyes, skin, and respiratory mucosa, and can also cause cancer in high concentration (Zhu et al., 2017a; Liu et al., 2018a). Atmospheric HCHO is an intermediate product of almost all volatile organic compounds (VOCs) oxidation, it can be therefore indicative of the overall VOCs level (Chan et al., 2019). HCHO can also be emitted through anthropogenic sources, biogenic sources, and biomass combustion. Anthropogenic sources like transportation, power, industry, and residential etc. increase the amount of HCHO by emitting VOCs into the atmosphere (Wang et al., 2017). In addition, biogenic volatile organic

compounds (BVOCs) are also important sources of HCHO. Isoprene emitted by plant can be oxidized to generate HCHO, which causes the concentration of HCHO in some lush vegetation areas to be largely affected by emission of BVOCs (Millet et al., 2008). The removal of HCHO is mainly through photolysis, reaction with OH radicals and the deposition (Ling et al., 2016; Xing et al., 2020).

Satellite remote sensing can achieve large-scale observation of atmospheric pollutant gases including HCHO, which has been widely used in recent years. Sensors currently available for HCHO observation include the Global Ozone Monitoring Experiment (GOME) on ERS-2 (Burrows et al., 1999; Martin et al., 2004b), Scanning Imaging Absorption Spectrometer for Atmospheric Chartography (SCIAMACHY) on ENVISAT (Bovensmann et al., 1999; Stavrakou et al., 2009), Ozone Monitoring Instrument (OMI) on Aura (Levelt et al., 2006; Zhu et al., 2017b), GOME-2 A, B, and C on METOP as the successor of GOME (Callies et al., 2000; De Smedt et al., 2012), Ozone Mapping and Profiler Suite (OMPS) on Suomi-NPP (Su et al., 2019), and Tropospheric Monitoring Instrument (TROPOMI) on Sentinel-5P (Veefkind et al., 2012; Vigouroux et al., 2020). OMI can provide daily data of HCHO with higher spatial resolution (13 km×24 km). As a new generation of sensors, TROPOMI was launched in 2017, it has better spatial resolution (7 km×7 km) but lacks long-term observation so far. It would be an advantageous tool of satellite remote sensing to achieve more detailed analysis in the future (Veefkind et al., 2012).

Previous studies reported satellite observed long-term and large-scale distribution and variation of HCHO in China and all over the world (Millet et al., 2008; Zhu et al., 2017a; Liu et al., 2020). Twelve years observation of multi-satellite (OMI, GOME-2, SCIAMACHY) showed that the trend of HCHO vertical column densities (VCDs) over eastern China is consistent with that of anthropogenic VOCs (Shen et al., 2019). Based on 10 years observation of OMI HCHO, Liu et.al (2018a) indicated that high HCHO VCDs in tropical forests region are greatly affected by biomass burning and meteorological factors including temperature and precipitation. In addition, the ground-based remote sensing can also be available for HCHO observation, such as the multi axis differential optical absorption spectroscopy (MAX-DOAS) measurement. The vertical distribution of HCHO derived from MAX-DOAS measurement was characterized by the higher HCHO concentrated near the surface (Lee et al., 2015; Chan et al., 2019). By employing the box model, Li et al. (2014) found that isoprene oxidation initiated by OH radicals have a great contribution to the HCHO formation in semi-rural region of the Pearl River Delta (PRD) in China.

HCHO participates in the complex photochemical reaction of NO_x (NO_x= NO + NO_2) and directly affects the production of O_3 in troposphere. Due to the short lifetime of HCHO and NO_2, their spatial distributions were greatly affected by local emission of VOCs and NO_x, which received widespread attention as precursors of tropospheric O_3 (Zaveri et al., 2003; Chan et al., 2019). Consequently, HCHO and NO_2 can be assumed as indicators of VOCs and NO_x, and the ratio of formaldehyde to nitrogen dioxide (HCHO/NO_2, FNR) can be an indicator to analyse the O_3 formation regime (Sillman, 1995; Martin et al., 2004a; Schroeder et al., 2017). For instance, by using FNR from long-term OMI HCHO and NO_2 data, O_3 sensitivity of the United States was evaluated. O_3 formation regime can be designated as VOC-limited for FNR < 1, NO_x-limited for FNR > 2, and transition for 1 < FNR < 2, which serves as the transitional regime between VOC-limited and NO_x-limited regimes,

indicating the production of O_3 can be changed by both VOC and NO_x (Duncan et al., 2010). In view of China, OMI products over three representative regions (North China Plain (NCP), the Yangtze River Delta (YRD) and the PRD) were investigated, revealing that the O_3 formation regime varied in both time and space, and the contribution of emission sectors to precursors changed with the type of regimes (Jin and Holloway, 2015). During special events such as Asia-Pacific Economic Cooperation in 2014 and Grand Military Parade in 2015, FNR in Beijing had become higher compared with previous periods, and the O_3 formation regime shifted toward NO_x-limited regime with control strategies (Liu et al., 2016).

In this study, OMI satellite data were used to investigate the temporal and spatial distribution characteristics of atmospheric HCHO in Shanghai from 2010 to 2019, combined with meteorological data and emission inventories to analyse the influencing factors. FNR calculated by satellite HCHO and NO_2 were applied to capture variation of the O_3 formation regime in Shanghai over the past decade. Considering that satellite data only reflect the column density of trace gas around overpass time, hourly surface FNR and O_3 concentration increment were proposed to correct the satellite FNR, so that it can better indicate O_3 formation in ~~a~~the daytime.

2 Data and Methods

2.1. Satellite data

OMI on Aura orbits the earth in about 98 minutes, which can achieve full coverage of the earth in one day. It overpasses at 13:45 local time (LT) each day. The scanning width is 2600 km, and is divided into 60 rows~~pixels~~. The sensor contains 3 channels, including UV-1, UV-2, and VIS, with a wavelength coverage of 264-~~-~~504 nm. This band allows to observe a variety of trace gases, e.g., HCHO, NO_2, and SO_2 (Zhang et al., 2019). The retrieval algorithm of this product is based on nonlinear least-squares fitting which get slant column density (SCD) as the result. Then SCD can be converted to VCD through Air Mass Factors (AMF). The Level-2 OMI HCHO product OMHCHO Version-3 is used in this study (https://disc.gsfc.nasa.gov). Since atmospheric HCHO is mainly distributed in the troposphere, the total VCD can be regarded as the tropospheric VCD of HCHO (Duncan et al., 2010). The Level-2 OMI NO_2 product OMNO2.003 Version-4 is adopted as tropospheric NO_2 VCD in this study (https://disc.gsfc.nasa.gov).

2.2. Methodology

In this study, Shanghai and surrounding areas were gridded into to a spatial resolution of 0.01°×0.01°, then HCHO VCD of each pixel was assigned to the respective grid by determining the coordinates information. Weight function including cloud function and pixel size was introduced to effectively improve the quality of processed data (Xue et al., 2020). In order to remove~~ensure~~ data with poor quality as much as possible, HCHO data with cloud fraction ≤ 30%, solar zenith angle ≤ 70°, and Main Data Quality Flag = 0 were selected in this study. In addition, the quality of pixel data with large size is poor, so 5 marginal pixels on each side were abandoned, and only pixel data within 6~55 were selected (Zhu et al., 2017a; Xue et al., 2020). Because OMI has experienced row anomaly since 2007, Xtrack flag = 0 was required to eliminate the influence of

poor quality data affected by row anomaly (http://projects.knmi.nl/omi/research/product/rowanomaly-background). As HCHO satellite data have large error, fitting root mean square (RMS) ≤ 0.003 was limited to remove most outliers (Souri et al., 2017). The selection of NO_2 satellite data was basically the same as that of HCHO, but without fitting RMS parameter filtering, and cloud radiance fraction ≤30% was required (Krotkov et al., 2016). ~~After filtering, the pixel data were gridded to the spatial resolution of 0.01°× 0.01° for further discussion (Xue et al., 2020).~~Moreover, the linear regressions of monthly deseasonalized zonal mean HCHO VCDs with 0.5° latitude steps over remote pacific region (29° - 33 °N, 160° - 140 °W) indicated that OMI HCHO product used in this study do not show the obvious drift (Zhu et al., 2017b).

2.3. Auxiliary data

The meteorological data, including monthly temperature, sunshine hours, precipitation, and relative humidity are acquired from the National Bureau of Statistics of China (http://www.stats.gov.cn/). Hourly temperature data at Shanghai Hongqiao INTL Site (31.20°N, 121.34°E) come from the National Climatic Data Center (NCDC, https://www.ncdc.noaa.gov/). The anthropogenic sources of HCHO in Shanghai are calculated based on the ~~China~~ Multi-resolution Emission Inventory for China (MEIC, http://www.meicmodel.org/). Surface HCHO and NO_2 concentrations were measured by long-path differential optical absorption spectroscopy (LP-DOAS) at the Jiangwan campus of Fudan University in Shanghai (31.34°N, 121.52°E). The O_3 data of Qingpu Dianshan Lake Site (31.09°N, 120.98°E) and Hongkou Site (31.30°N, 121.47°E) in Shanghai are obtained from the Shanghai Environmental Monitoring Center (http://www.semc.com.cn/aqi/Home/Index).

3. Results and Discussion

3.1. The temporal and spatial variation of HCHO

HCHO VCDs for annual, monthly and seasonal variations in Shanghai from 2010 to 2019 are shown in Fig. 1. HCHO VCDs decreased from the highest value of 12.29×10^{15} molec·cm^{-2} in 2010 to the lowest value of 9.97×10^{15} molec·cm^{-2} in 2012, then rebounded from 2012 to 2014, and fluctuated slightly in the following years (Fig. 1a). The column value and variation are similar to previous study in the YRD, China (Zhang et al., 2019). Before 2018, the high-VCD concentrated in June to August for about 15×10^{15} to 20×10^{15} molec·cm^{-2}, the low-VCD appeared in January to February and November to December for about 3×10^{15} to 9×10^{15} molec·cm^{-2}, and VCDs were comparable in remaining months (Fig. 1b). In addition, the amplitude of monthly HCHO VCDs was relatively smaller in 2018 and 2019, and mainly concentrated from 6×10^{15} to 15×10^{15} molec·cm^{-2}. The HCHO VCDs varied with the season, the maxima and minima corresponding to the respective summer (June, July and August) and winter (December, January and February), whereas moderate levels in spring (March, April and May) and autumn (September, October and November) (Fig. 1c). Previous MAX-DOAS and OMI observations also exhibited the same seasonal patterns of HCHO in the YRD, China (Jin and Holloway, 2015; Chan et al., 2019). High temperature and abundant radiation are conducive to the plant growth to produce BVOCs and the photochemical reaction of

VOCs, which boost the HCHO formation in summer (Sharkey and Loreto, 1993; Duncan et al., 2009; Narumi et al., 2009). Thus, HCHO VCDs would be relatively low in winter under the opposite weather conditions.

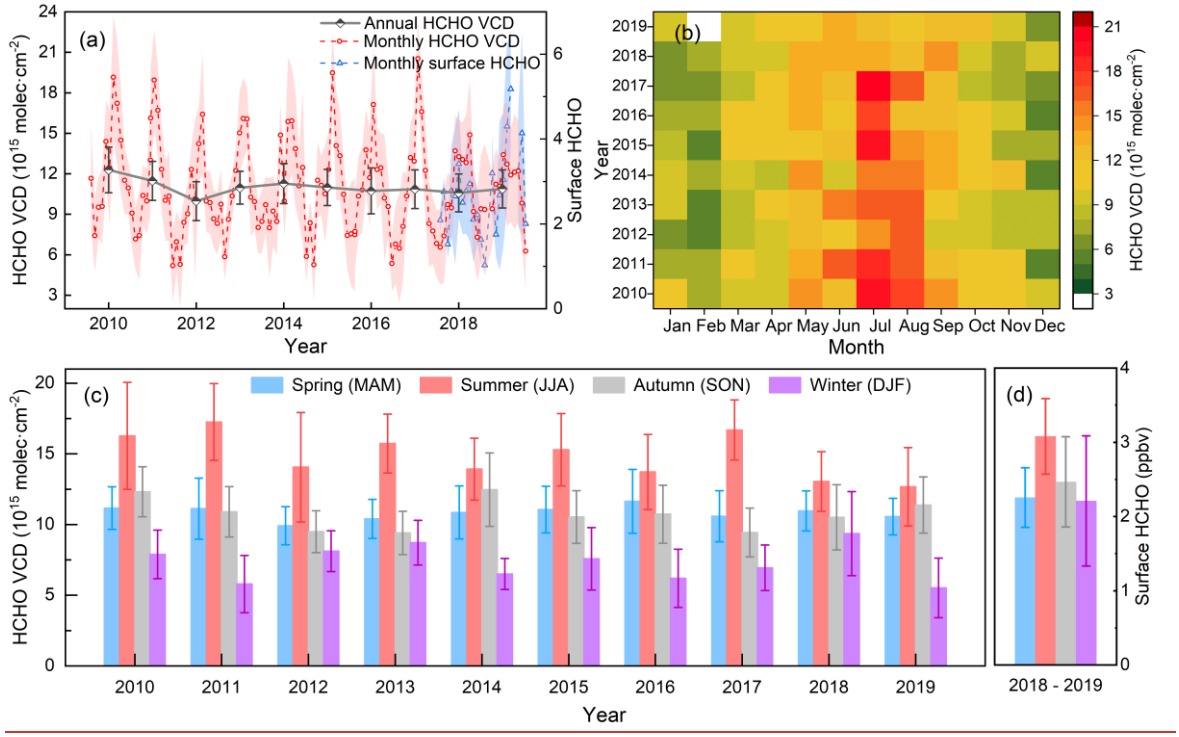

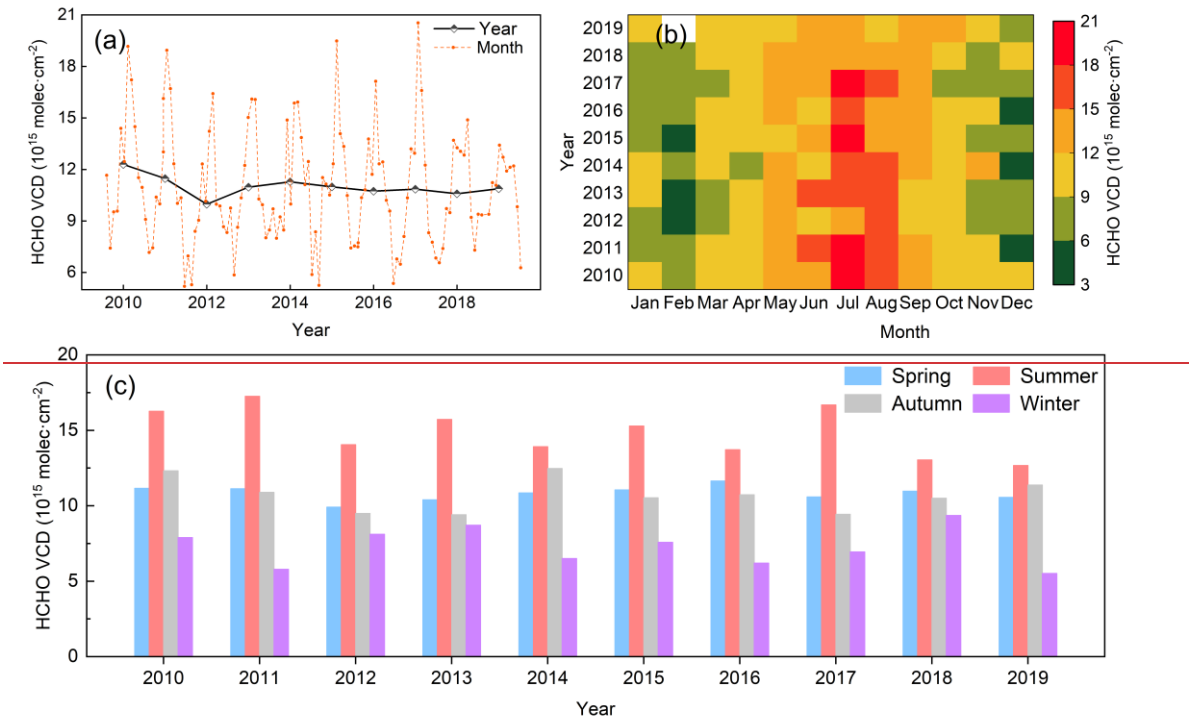

Figure 1. OMI and LP-DOAS observed time series of HCHO in Shanghai. ~~VCDs for~~ (a) ~~annual, (b) monthly and~~to (c) reflect the annual, monthly and seasonal variations of HCHO VCD~~in Shanghai~~ during 2010-2019.~~,~~ (d) reflects the seasonal variation of surface HCHO during 2018-2019.

The HCHO VCDs within 10 km of LP-DOAS measurement site were averaged to compare with the surface HCHO between 13:00 and 14:00 (Fig. S1). It shows that HCHO VCDs and surface HCHO concentrations are not consistent very well, as HCHO is not completely concentrated near the ground, but has a high concentration at higher altitudes (Chan et al., 2019; Wang et al., 2019). Spatial heterogeneity of surface HCHO in horizontal can also impact the consistency of the comparison. However, the surface HCHO observed by LP-DOAS shows the same seasonal characteristics as HCHO VCDs (Fig. 1d).

The spatial distribution of 10-year averaged HCHO VCD was given in Fig. 2a. In general, HCHO VCDs in eastern coastal area were relatively low, with the level of about 10×10^{15} molec·cm^{-2}. While those in western regions adjacent to other provinces were relatively higher, about 13×10^{15} molec·cm^{-2}. Noted that area with the highest HCHO VCD in Shanghai not appeared in the city center (marked by the red box) but in the relatively remote Qingpu (QP) district, followed by Songjiang (SJ) and Jinshan (JS) district. Compared to the anthropogenic Non-methane volatile organic compounds (NMVOCs) emissions, the distribution of HCHO VCDs does not show the same spatial pattern (An et al., 2021). The high HCHO in western Shanghai were frequently observed and may be explained by the transport of air masses containing high concentrations of reactive VOCs sometimes from Zhejiang and Jiangsu provinces and the significant contribution of local biogenic isoprene to HCHO (Su et al., 2019; Zhang et al., 2020; Zhang et al., 2021).

Figure 2b shows the difference of HCHO VCDs between 2019 and 2010. It suggests that except for the eastern and southern coastal areas, as well as the eastern area of Chongming Island, HCHO VCDs in Shanghai showed an overall downward trend during the past 10 years, with Qingpu district experiencing the largest decline. Figure 2c to Fig. 2f display the spatial distribution of HCHO VCDs in different seasons. HCHO VCD in summer was basically above 12×10^{15} molec·cm^{-2}. In winter, the value was around 7×10^{15} molec·cm^{-2} for most regions except for Qingpu district. While in spring and autumn, it was in the moderate level of about 10×10^{15} molec·cm^{-2}. The spatial distribution of HCHO VCDs in different seasons was similar to the 10-year averaged characteristics of high-value in the west and low-value in the east.

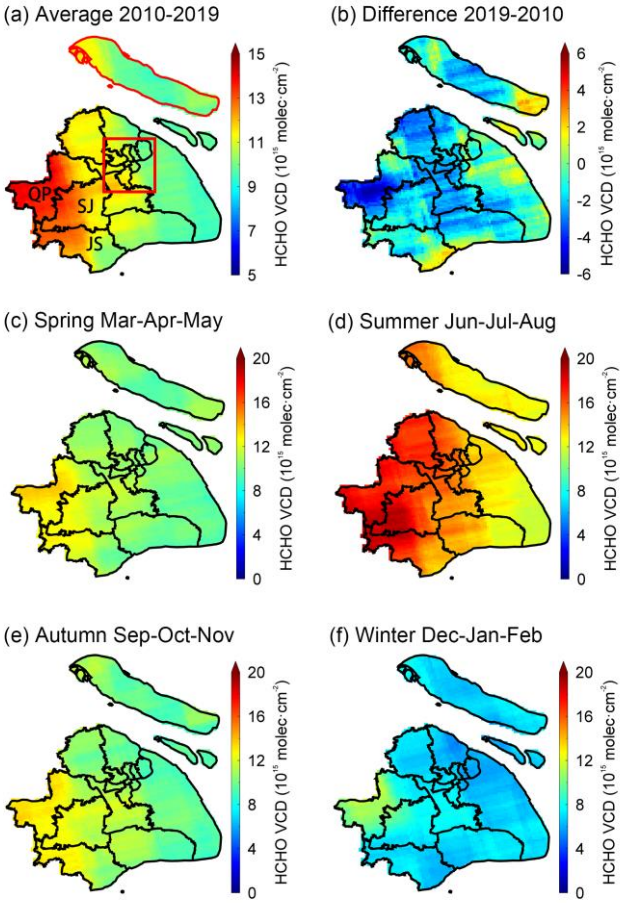

Figure 2. Spatial distribution of HCHO VCDs in Shanghai: (a) average HCHO VCD for 10 years, (b) the difference of HCHO VCDs between 2019 and 2010 (2019 minus 2010), and (c) to (f) for different seasons. In Fig. 2a the city center is marked with red box, Chongming Island is displayed with red boundary, QP, SJ, and JS refer to Qingpu, Songjiang, and Jinshan district.

3.2. Influencing factors

The relationship between monthly ~~-~~HCHO VCDs~~Figure 3 shows the monthly averaged HCHO VCDs~~ and meteorological variables~~parameters,~~ including temperature, sunshine hours, precipitation, and relative humidity were analysed via the linear

regression.~~from 2010 to 2018.~~ The stepwise regression results show that only temperature correlated with HCHO VCDs significantly ~~A~~among these four meteorological factors. The linear regression of temperature contribution and HCHO VCD was shown in Fig. 3. The temperature contribution has a good correlation with the observed HCHO VCD (R^2 = 0.72), which means that temperature can explain about 72% of the variation of HCHO VCD. The remaining part that cannot be explained by temperature appears in the form of residual, which is considered as the influence of other changing factors such as anthropogenic emissions (Li et al., 2019). The residual in summer in some years would be particularly large, which indicates that in addition to temperature, there are other factors affecting HCHO VCD significantly.

~~, temperature had the most significant correlation with HCHO VCDs. Considering the daily averaged temperature was used here while HCHO VCDs observed by satellite only reflect the level at 13:45, the correlation between HCHO VCDs and temperature at 14:00 was further analysed, which demonstrated that the strong Pearson correlation coefficient is 0.842 at 0.01 level. It can be inferred that temperature is an important influencing factor of HCHO. The variation of sunshine hours from January to May was similar to that of HCHO VCDs. The reason for the positive effect of temperature and sunshine hours on HCHO VCDs is same as that mentioned in seasonal characteristics. It also implies indirectly the role of biogenic emissions in HCHO, which is favored by the high temperature and sunshine hours (Millet et al., 2008; Duncan et al., 2009).~~

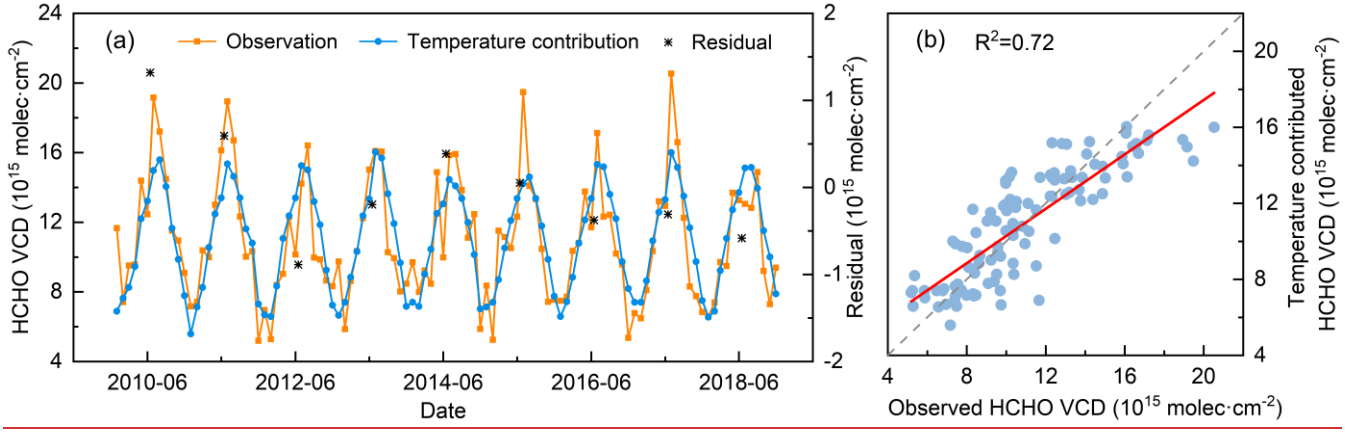

Figure 3. Monthly HCHO VCDs and the temperature contribution in Shanghai during 2010-2018. (a) reflects the temporal variations and (b) illustrates the correlation analysis. The black points represent the annual average residuals.

The precipitation and relative humidity reached peak in June, while the sunshine hours reached the dip, and HCHO VCD declined with the temperature rose (Fig. S2). Shanghai has a subtropical monsoon climate with rain and heat in the same period. Abundant precipitation largely favoured the wet deposition of HCHO and offset the impact of rising temperature, resulting in a small decrease in HCHO VCDs in June (Pang et al., 2009). The result of Fisher's exact test also illustrates that when the relative humidity changes remarkably, the variation of HCHO VCDs in summer would be significantly affected ($P < 0.05$).

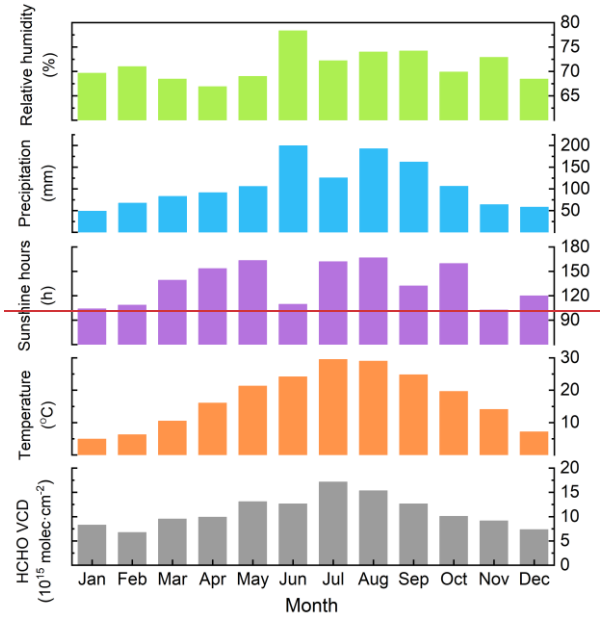

~~**Figure 3. HCHO VCDs and meteorological factors including temperature, sunshine hours, precipitation and relative humidity in Shanghai for 2010-2018.**~~

To explore the impacts of anthropogenic sources on HCHO abundance, primary emissions and secondary productions of HCHO from anthropogenic sources were estimated. NMVOCs emissions from MEIC v.1.3 grid inventories for the year of 2010, 2012, 2014, and 2016 were mapped to SAPRC07 mechanism species~~were used~~. Primary HCHO was directly obtained from the inventory, secondary HCHO production was calculated based on 1-day HCHO yields of several NMVOCs under high-NO_x condition (Table S1) (Shen et al., 2019).

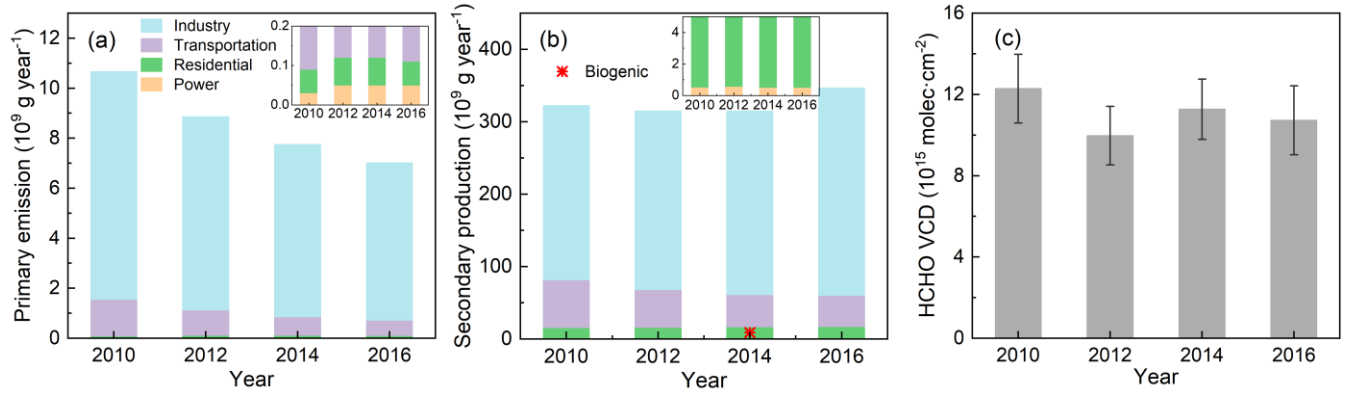

Figure 4. Primary and estimated secondary production of HCHO from anthropogenic NMVOCs, biogenic contribution of HCHO in 2014 was marked as red cross in Figure 4(b).

~~HCHO emission inventory was calculated by the SAPRC07 chemical mechanism and MEIC VOCs inventory for different sectors of traffic, industrial, power and residential over these years.~~ In Fig. 4a and 4b, for the total of primary emissions and secondary productions, the contribution~~emission~~ of industrial sector was much higher than other sectors, accounting for about ~~87.9~~79.3% of the total, followed by transportation sector, accounting for about ~~10.8~~15.7% ~~(Fig. 4)~~. Residential and power sectors were far lower, the proportions over these years ~~was~~ were basically less than ~~1~~5%. As major sectors, the contribution~~emission~~ of industrial ~~and transportation~~ increased 17.2%, while the contribution of transportation decreased about 3~~0~~.2~~9~~% ~~and 58.5% respectively~~. ~~In addition, the total anthropogenic emission of HCHO dropped 34.2% in 2016 compared with that in 2010, which was basically consistent with the total decrease in HCHO VCDs. It indicates that strengthening the control of industry and transportation should be an effective tactic for alleviating HCHO pollution.~~ The primary emission of HCHO keeps decreasing (about 34.2% compared to 2010), while secondary produced HCHO did not change significantly. Furthermore, the changes and proportional relationships between primary emission and secondary production of HCHO for these sectors are different, which means the VOCs source profile of different emission sectors would affect the amount of secondary HCHO production.

In addition, HCHO produced by biogenic sources in 2014 was also calculated, and the BVOCs emissions were referred from Liu et al. (Liu et al., 2018b; 2018c). HCHO yield from BVOCs emission was about 9.07×10^9 g, which is much smaller compared with anthropogenic contribution, indicating that the anthropogenic is the main contributor of secondary production of HCHO in Shanghai (Shen et al., 2019; Fan et al., 2021).

Fig. 4c shows that the annual trend of HCHO VCDs is not synchronized with that of primary or secondary HCHO. It means that, besides the combined effect of the primary and secondary source, the changes of HCHO VCDs should also be affected complexly by various factors. In addition, it should be noted that HCHO yield from VOCs is proportional to NO_x condition (Palmer et al., 2006; Marais et al., 2012; Miller et al., 2017). With context of the continuous NO_x decreases in Shanghai, the estimation using a fixed HCHO yield may overestimate secondary HCHO production in later years (Xue et al., 2020). However, the NO_x concentration in Shanghai (basically 30-60 ppbv in urban) is still much higher than the defined high NO_x condition (1 ppbv) in previous studies (Gao et al., 2017). Therefore, in such a high NO_x condition, the effect of NO_x decreases on HCHO yield needs to be further studied.

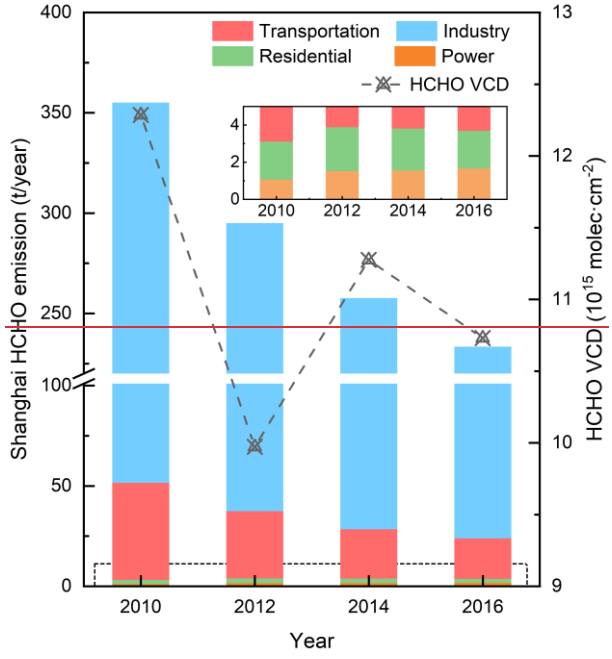

225

~~Figure 4. The variation of HCHO emission from anthropogenic sources including transportation, power, residential and industrial sectors.~~

3.3. FNR and O_3 formation regime

As the important precursors of O_3, HCHO and NO_2 can be served as indicators for VOCs and NO_x. On this basis, the 230 HCHO/NO_2 ratio from satellite observation (FNR_{SAT}) can be employed to identify the O_3 formation regime. The variations of monthly averaged VCDs of HCHO, NO_2, and FNR_{SAT} in Shanghai over the past 10 years are given in Fig. 5. NO_2 VCDs were featured by the highest in winter and the lowest in summer, which was opposite to HCHO and fluctuated more fiercely. The peaks were mainly on account of its longer lifetime in winter (Zhang et al., 2007). While in summer, the adequate sunlight and precipitation accelerated the photochemical removal and wet deposition of NO_2, resulting in the dip (Wang et 235 al., 2018; Xue et al., 2020). FNR_{SAT} also exhibited the obvious annual cycle of high in summer and low in winter. According to the criteria proposed by Duncan et.al (2010), O_3 formation regime in Shanghai was usually under NO_x-limited from June to August, and controlled by VOC-limited and transition regime for the rest of months. From May to September in 2014, Shanghai all under NO_x-limited regime, and FNR_{SAT} reached the highest value over the past 10 years. In 2019, the value of monthly FNR_{SAT} fluctuated gently, which showed the trend moving towards the transition regime threshold of 1-2.

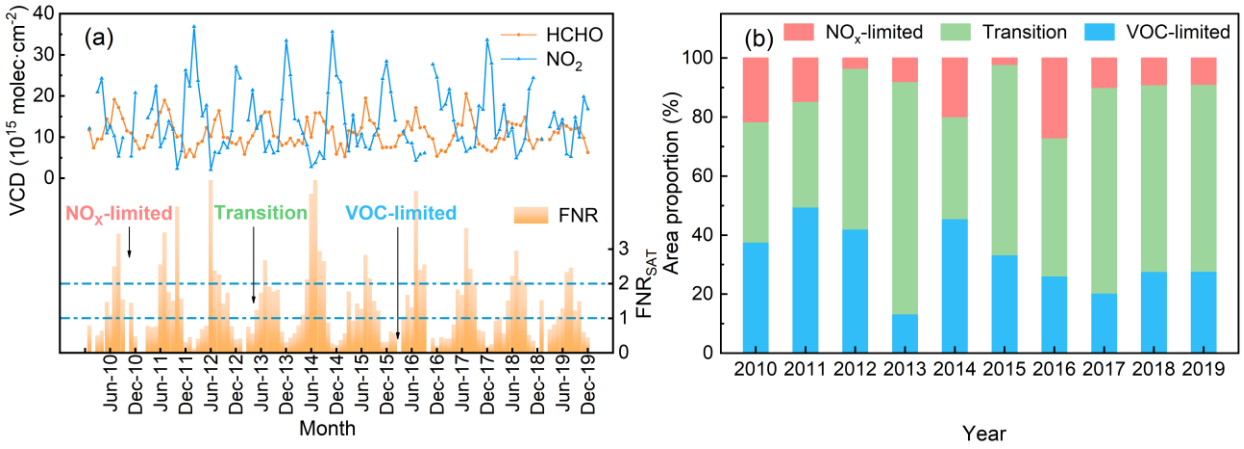

Figure 5. Temporal and spatial variation of FNR_{SAT} in Shanghai: (a) variations of HCHO, NO_2 and FNR_{SAT} from 2010 to 2019, and (b) the area proportion for different O_3 formation regimes in these years.

The spatial distribution of FNR_{SAT} in Shanghai is presented in Fig. 6. Comparing FNR_{SAT} in 2019 with that in 2010, the NO_x-limited regime in the western Shanghai transformed into transition regime, and VOC-limited regime in the northern Chongming Island almost completely became transition regime. It manifests itself in the reduction in the NO_x-limited and VOC-limited regimes while the increase in the transition regime. Referring to previous study on the variation of NO_2 VCDs spatial distribution in Shanghai observed by satellite, this phenomenon may be related to the spatial characteristics of concentration variations of two precursors (Xue et al., 2020). This result is also reflected in Fig. 5b. In the past 10 years, the proportion decreased from 37.6% to 27.7% for VOC-limited area, and from 21.6% to 8.9% for NO_x-limited area, respectively. Meanwhile, the transition regime area increased from 40.8% to 63.3%. Xu et al. (2019) suggested that O_3 formation regime in Shanghai trend to transform from VOC-limited regime to NO_x-limited regime after 2020 through WRF-Chem model simulation. In this study, the increase of transition regime may be the transition state from VOC-limited to NO_x-limited regime.

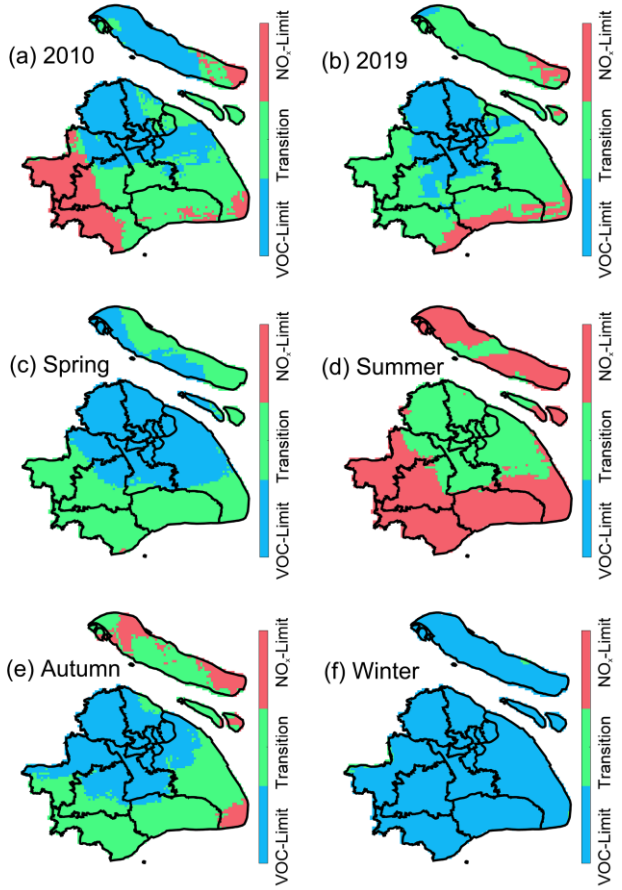

Figure 6. The spatial distribution of FNR_{SAT} for (a) 2010, (b) 2019, and (c) to (f) different seasons in Shanghai.

Figure. 6c to Fig. 6f show the spatial distribution of FNR_{SAT} for different seasons during the decade. In spring, the northern area of Shanghai was VOC-limited regime while the southern area was transition regime. From spring to summer, the VOC-limited area almost transformed into transition regime, and the transition regime nearly turned into NO_x-limited at the same time, which mainly caused by the increase of HCHO and the decrease of NO_2. The distribution in autumn was similar to that in spring. In winter, Shanghai was basically under VOC-limited. In the light of the temporal and spatial distribution of O_3 formation regime inferred by FNR_{SAT}, the emission reduction measures for O_3 precursors would be more rationally.

Besides, there are differences in O_3 formation regime in urban and ~~rural~~suburban areas of Shanghai, with the main manifestation that the central urban area was inclined to be in VOC-limited regime and the ~~rural~~suburban area was more likely to be in NO_x-limited regime. In order to analyse the differences in more detail, area within 10 km around the Jiangwan campus of Fudan University was selected to represent the urban area (about 12 km to the city center), and equally sized area around Dianshan Lake (31.09°N, 120.98°E) of Qingpu district was regarded as the ~~rural~~suburban area (about 50 km to the city center), respectively. Since O_3 pollution is relatively serious from April to September, this period can be chosen as a research case. The maximum 8-hour average concentration of O_3 at the Hongkou and the Qingpu Dianshan Lake Site were

used to characterize O_3 concentration in urban and ~~rural~~suburban areas. NO_2 VCDs in urban area were higher than that in ~~rural~~suburban, while HCHO VCDs presented the opposite character (Fig. 7a). The lower NO_2 in ~~rural~~suburban area was associated with the less NO_x emission than that in urban, corresponding to the larger FNR_{SAT}. From Fig. 7b, the O_3 production was under transition regime in ~~rural~~suburban area except for 2016, while VOC-limited regime occupied for most years in urban area. The O_3 concentration in ~~rural~~suburban area was always higher than that in urban (Fig. 7c). In this study, transition regime in ~~rural~~suburban for most years led to higher O_3 concentration correspondingly (Jin et al., 2020). In addition, high concentration of NO_x in urban area may lead to titration of O_3 by NO, which would also cause the lower O_3 concentration in urban (Geng et al., 2008; Duncan et al., 2010).

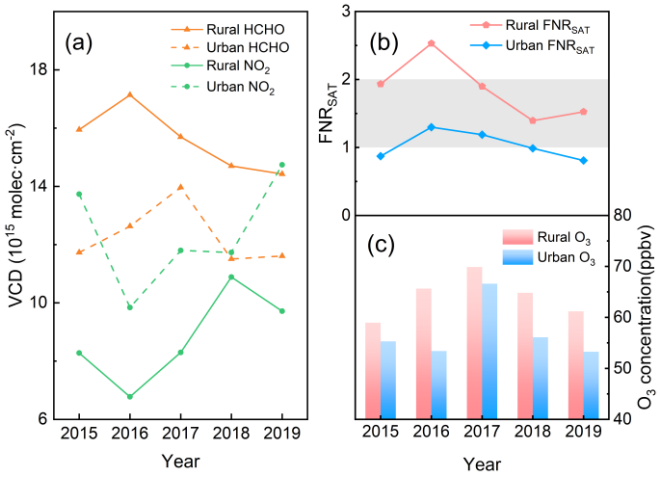

Figure 7. Differences of (a) satellite observation of HCHO and NO_2 VCDs, (b) FNR_{SAT} and (c) surface O_3 concentration in urban and ~~rural~~suburban areas of Shanghai from 2015 to 2019.

3.4. Correction of FNR_{SAT}

FNR is originally proposed as an indicator to characterize the sensitivity of the instantaneous O_3 production rate (Duncan et al., 2010). Satellite observation only reflects the averaged column of the trace gases around overpass time, so the FNR_{SAT} may not accurately infer the surface O_3 formation regime during the day (Duncan et al., 2010; Jin and Holloway, 2015; Jin et al., 2017). FNR_{SAT} was compared with FNR_{LP} at the satellite overpass time on the monthly and daily scales. Results show that FNR_{SAT} and FNR_{LP} were consistent well on monthly scale (R^2=0.95, between April and August), but they were quite different on the daily scale, and the relationship was easily affected by the boundary layer height (BLH) and other factors (Schroeder et al., 2017).

As shown in Fig. 8a to Fig.8c, LP-DOAS observation ~~provides~~ provided ~~surface concentration of O_3 precursors~~FNR_{LP} with the high temporal resolution throughout the day, ~~therefore~~ and ~~FNR observed by LP-DOAS (~~FNR_{LP}~~)~~ was in good agreement with hourly O_3 concentration. It means that FNR_{LP} should be a good indicator~~more suitable~~ to distinguish the formation regime of surface O_3 on a detailed time scale. In addition, the highest value of FNR_{LP} at noon means that FNR_{SAT} at overpass

time approximately close to the highest level in a day. Thus, it would be valuable to introduce the time series of FNR_{LP} to make FNR_{SAT} better reflect the characteristic of O_3 formation during the daytime.

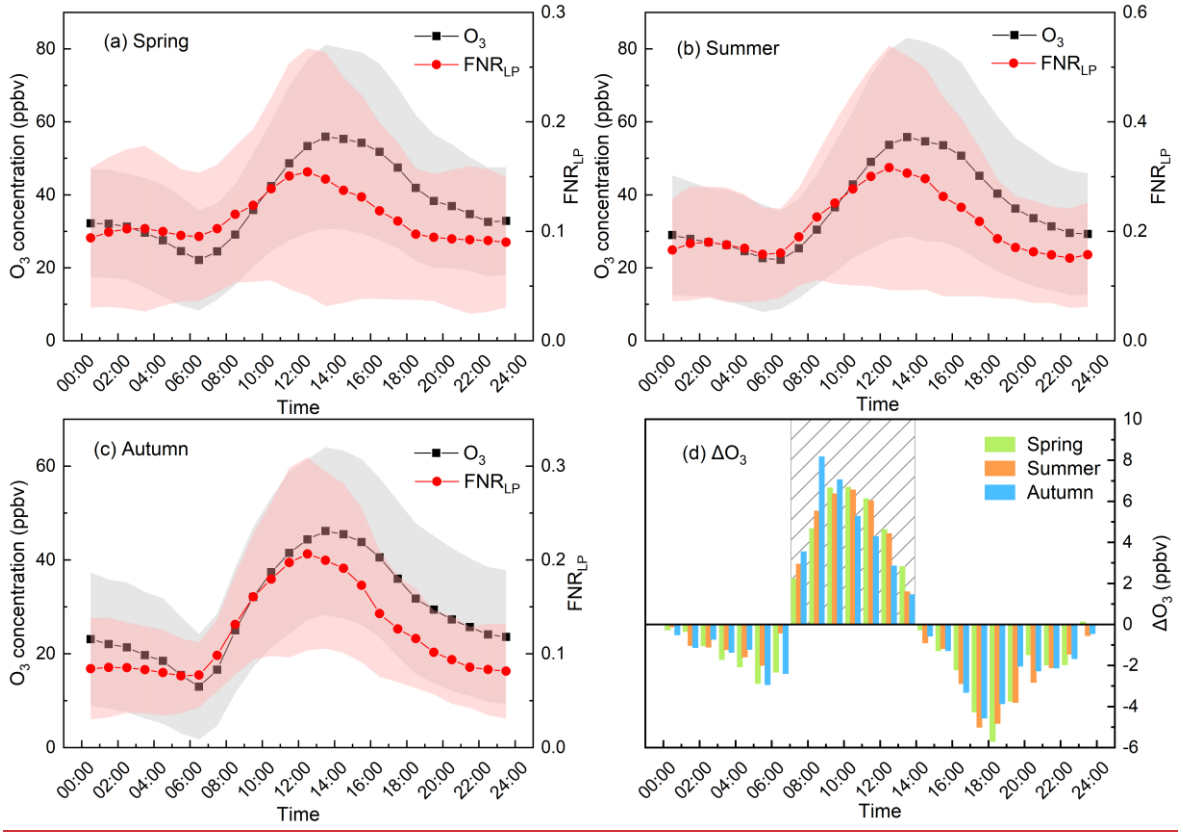

Figure 8. Diurnal variations of FNR_{LP}, O_3 and ΔO_3 for spring, summer and autumn during 2018-2019. ΔO_3 represents increment of hourly O_3 concentration, as referred to Eq. (3). The shaded area in (d) represents the period when ΔO_3 greater than 0.

~~Here FNR_{SAT} and FNR_{LP} were compared together as the function of surface O_3 concentration. Only FNR_{LP} from 08:00 to 18:00 LT were considered owing to the relatively strong photochemical reaction of O_3 formation for this period. FNR_{SAT} was spatially averaged for grids within 10 km of the LP-DOAS measurement site. Then,~~ Tthree cases during the LP-DOAS observation at the Jiangwan campus of Fudan University were selected for the further discussion under the criteria of the hourly concentration of O_3 exceeding 200 μg/m^3 (secondary concentration limit stipulated in ambient air quality standards of China, GB 3095-2012). In Fig. ~~8a~~ 9a and Fig. ~~8c~~9c, the upward trend in FNR_{LP} as the O_3 concentration increases means that the formation of O_3 was under VOC-limited regime in Case 1 and 3. VOC-limited and transition regimes caught in Case 1 through FNR_{SAT} were different from that identified by FNR_{LP}. In Case 3, the O_3 formation regime remained in VOC-limited regime, which was the same as FNR_{LP}. As shown in Fig. 8b, FNR_{LP} indicated that the O_3 formation regime switched between three regimes in Case 2. As O_3 concentration increasing, the growth of FNR_{LP} at beginning indicated VOC-limited regime, while the subsequent slow variation suggested transition regime. When O_3 concentration reached maximum, FNR_{LP} got

smaller, which referred to NO_x-limited regime. But FNR_{SAT} only captured the VOC-limited and transition regime in Case 2. According to the results above, it is feasible and necessary to correct FNR_{SAT} to better represent the sensitivity of surface O_3 formation. Due to the less O_3 pollution in winter, FNR_{SAT} was only corrected for the remaining three seasons.

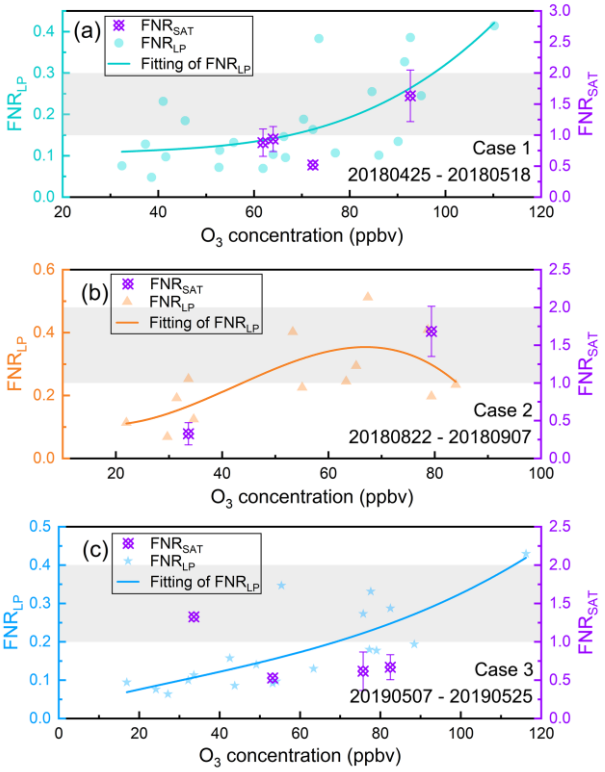

Figure ~~8~~9. Comparison of FNR_{SAT} and FNR_{LP} in three O_3 pollution cases. The curves are polynomial fit of FNR_{LP}, and the points are FNR_{SAT} in corresponding cases, the gray area indicates the transition regime for FNR_{SAT}. Only LP-DOAS measured data between 08:00-18:00 LT were contained.

~~As shown in Fig. 9a, the highest value of FNR_{LP} at noon means that FNR_{SAT} at overpass time approximately close to the highest level in a day. Therefore, we consider to utilize the ground surface FNR diurnal pattern observed by LP-DOAS during ozone polluted period to correct the FNR_{SAT}. It is noted that the ozone polluted period was defined as the duration with positive increment of hourly O_3 concentration, as referred to Eq. (3) and Fig. 9b, where can be seen that the ΔO_3 greater than 0 from 07:00 to 13:00 LT.~~

The correction of FNR_{SAT} was achieved through the following process. Firstly, the ratio of FNR at satellite overpass time to averaged FNR during O_3 pollution period (ΔO_3 greater than 0, i.e. 07:00 to 13:00 LT, referred to Fig. 8d) obtained from ground surface measurement was assumed to be same with that of satellite observation, which is expressed as:

$$\frac{FNR_{SAT}}{\overline{FNR}_{SAT}} = \frac{FNR_{LP,overpass\ time}}{\overline{FNR}_{LP}} \quad (1)$$

where $\overline{FNR}_{LP}$ is weighted average of FNR during O_3 pollution period observed by ground surface LP-DOAS measurement, $FNR_{LP,overpass\ time}$ is ground surface FNR observed at satellite overpass time. $\frac{FNR_{LP,overpass\ time}}{\overline{FNR}_{LP}}$ reflects the numerical relationship of FNR between satellite overpassed time and O_3 polluted period during a day, and can be serve as the correction coefficient to realize the correction for FNR_{SAT} on time scale to obtain the $\overline{FNR}_{SAT}$. Considering the relationship between time series of FNR and O_3 formation, ΔO_3 was involved to calculate the weighted average of FNR_{LP} ($\overline{FNR}_{LP}$) during 07:00 to 13:00 LT via Eq. (2), which can better indicate the ozone formation in a day.

$$\overline{FNR}_{LP} = \frac{\sum_{T=7}^{13} FNR_{LP,T} \times \Delta\Omega_{O3,T}}{\sum_{T=7}^{13} \Delta\Omega_{O3,T}} \quad (2)$$

$$\Delta\Omega_{O3,T} = \Omega_{O3,T} - \Omega_{O3,T-1} \quad (3)$$

Where $\Delta\Omega_{O3,T}$ is the increase of O_3 concentration at time T, $FNR_{LP,T}$ is the FNR_{LP} at time T. Moreover, variation characteristics of FNR_{LP} in different seasons (as shown in Fig. 8a to Fig. 8c) suggest that the correction of FNR_{SAT} should be discussed seasonally.

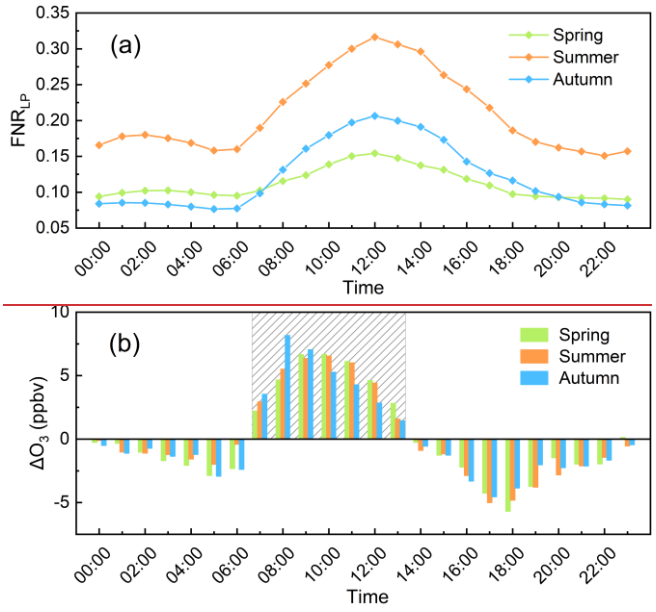

~~**Figure 9. Diurnal variations of (a) FNR_{LP} and (b) ΔO_3 for different seasons in 2018-2019. The shaded area represents the period when ΔO_3 greater than 0.**~~

Afterwards, the seasonal correction coefficients of 0.85, 0.84, and 0.77 were obtained for spring, summer, and autumn, respectively. It is noted that all the correct coefficients were less than 1 due to the FNR_{LP} value for OMI overpasses time relatively larger than other time. It would inevitably make the O_3 formation regime inferred by corrected FNR_{SAT} trend to be VOC-limited. There were 87 months with effective FNR_{SAT} in three seasons during 2010-2019 and the proportion of months for different regimes was listed in Table 1. Before the correction, the VOC-limited and NO_x-limited regimes, as well as

transition regime were almost accounted for about one-third of the total months. After the correction, both of months for VOC-limited and transition regimes increased. The months under VOC-limited regime increased by 25% particularly, while decreased about 32.1% for NO_x-limited regime. Jin et al. (2020) used O_3 exceedance probability as the indicator to analyse non-linear dependence of long-term surface O_3 concentration on precursor emissions, and determined the OMI $HCHO/NO_2$ under transition regime ranging from 3.2 to 4.1. These thresholds are significantly larger than the value proposed by Duncan et al. (2010), which has the equivalent effect as the use of correction factors less than 1 in this study.

Table 1. Variations in the number and proportions of months in 2010-2019 for each regime before and after the correction.

Regime	Before corrected	Percentage before corrected	After corrected	Percentage after corrected	Percentage of change
VOC-limited	28	32.2%	35	40.2%	25.0%
Transition	31	35.6%	33	37.9%	6.5%
NO_x-limited	28	32.2%	19	21.8%	-32.1%

In terms of spatial distribution, the O_3 formation regime after correction in different seasons is shown in Fig. 10. Compared with Fig. 6, part of the transition regime area in spring transformed into VOC-limited regime after the correction, VOC-limited regime obviously expanded and increased about 15.6%. Most area in Chongming Island transformed into VOC-limited regime. In summer, part of the NO_x-limited regime area transformed into transition regime, and the area of transition regime increased about 11.9%. In autumn, the NO_x-limited regime almost disappeared, and the proportion of the transition regime area also decreased significantly, for about 13.2%, while the proportion of the VOC-limited regime area increased about 22%. The O_3 formation regime in Chongming Island was basically under transition regime. Researchers also pointed that thresholds of criteria would be regionally dependent, so the local surface FNR and O_3 concentration should be introduced in satellite correction (Duncan et al., 2010; Jin et al., 2020).

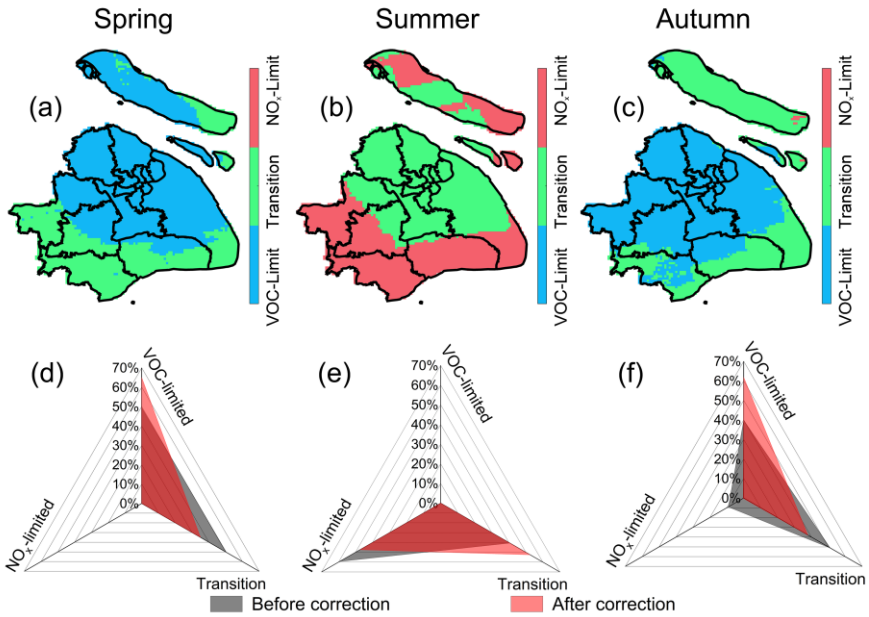

Figure 10. Spatial distribution of O_3 formation regime (upper row) and area proportion for each regime (bottom row) after correction for different seasons in Shanghai during 2010-2019.

In order to verify whether the correction of the satellite FNR improved the regime classification, O_3 formation regimes determined by satellite FNR before and after the correction were compared with that of surface observation. The variations of O_3 with surface HCHO and NO_2 have been plotted to determine the O_3 formation regimes from the surface observation (Figure 11). The daytime surface HCHO and NO_2 are from LP-DOAS measurements, and the O_3 observed by SP-DOAS (short-path DOAS), which is also located at Jiangwan campus of Fudan University, have been used with a high temporal resolution. O_3 formation regimes inferred from satellite FNR before and after the correction have also been marked in Figure 11 separately.

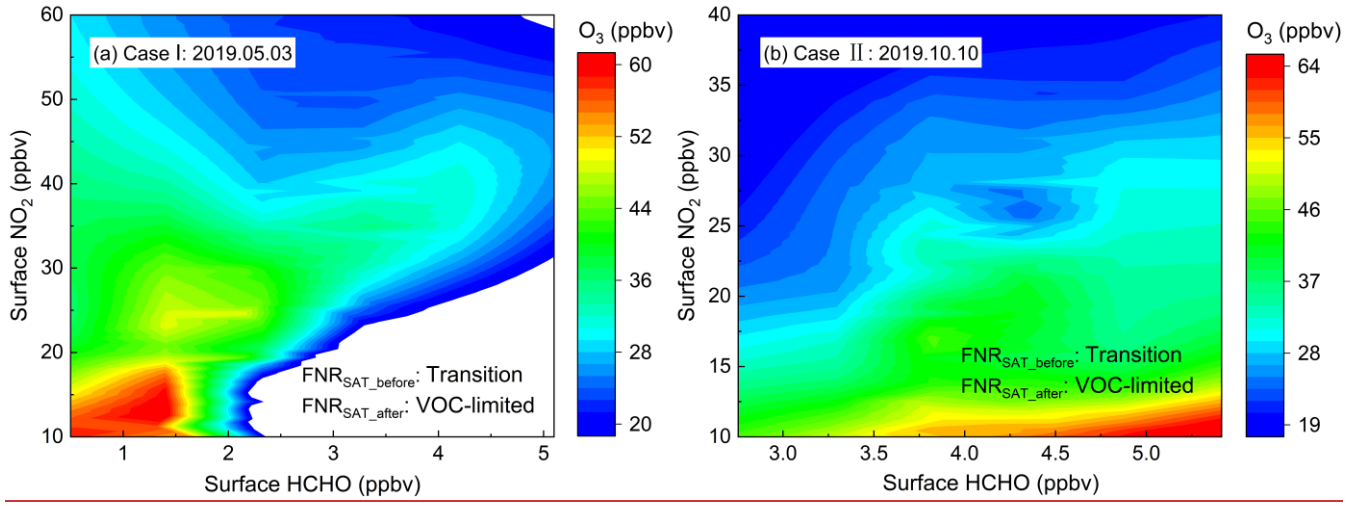

Figure 11. The variation of O_3 with surface HCHO and NO_2 for two cases of (a) May 3th, 2019 and (b) October 10th, 2019. $FNR_{SAT\ before}$ and $FNR_{SAT\ after}$ indicate the O_3 formation regimes inferred from the satellite FNR before and after the correction.

For Case I, O_3 decreases with the increase of NO_2, which can be attributed to the titration of O_3 by NO (Duncan et al., 2010). O_3 increased from top to bottom indicating it was under VOC-limited regime in Case I (Luo et al., 2020). For Case II, it can be seen that the high O_3 appeared with high HCHO and low NO_2, indicating it was under VOC-limited regime. The uncorrected satellite FNR indicated that these two cases were both under transition regime, while the corrected satellite FNR indicated they transferred to VOC-limited regime, which are consistent with the results of surface observation.

~~The O_3 formation regimes before and after the correction were compared with regime inferred by FNR_{LP} in Fig. 11. It can be seen from Fig. 9a that FNR_{LP} is significantly lower than 1, and it is not suitable for the threshold of FNR_{SAT} method to infer the O_3 formation regime. To infer the influence of precursors on O_3, linear regression was executed for precursors observed by LP-DOAS and O_3 concentration. O_3 formation regime was discerned by comparing the slopes versus HCHO and NO_2 (O_3-HCHO and O_3-NO_2: both positive reflect transition regime; positive and negative means VOC-limited; negative and positive suggests NO_x limited; both negative indicates titration of O_3 by NO and classified as VOC limited). In several months, LP-DOAS observation indicated VOC limited or transition regime, while the FNR_{SAT} reflected transition or NO_x limited regime, which mainly related to the high level of FNR at the overpass time of OMI. After the correction, the result of satellite was closer to LP-DOAS obviously,~~ It indicat~~es~~ing that the correction of FNR_{SAT} in this study can be considered to be ~~is~~ effective and make sense.

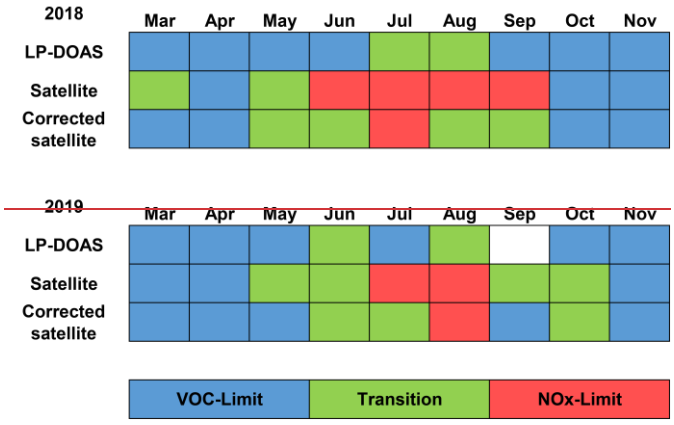

~~**Figure 11. The comparison of the observation results of the FNR_{SAT} and LP-DOAS on the O_3 formation regime in Shanghai 2018-2019 for each month except for winter. In each year, the top row represents the LP-DOAS observation result, the middle row represents the FNR_{SAT} observation before correction, and the bottom row represents the FNR_{SAT} observation after the correction.**~~

4. Summary and conclusions

Satellite data of OMI were used to study the temporal and spatial variation of HCHO in Shanghai from 2010 to 2019. HCHO VCDs fluctuated during the 10 years with obvious seasonal characteristics of highest value in summer, the lowest value in winter, and the moderate level in spring and autumn. In terms of spatial distribution, HCHO VCDs in western area were much higher than that in eastern coastal area. Compared with 2010, HCHO VCDs of Shanghai in 2019 showed an overall downward trend. As for the influencing factors, temperature ~~and sunlight~~ give the significant positive effect on HCHO VCDs while the abundant precipitation reduces HCHO in ~~atmosphere~~summer. Industry was an important contributor~~emission sector~~ of HCHO, and anthropogenic secondary production of HCHO occupied the main part of the HCHO source~~similarly showing a downward trend due to the government control~~.

In the past 10 years, O_3 formation regime changed toward transition regime gradually. O_3 formation regime in urban area was more likely to be VOC-limited regime, while regime in ~~rural~~suburban area was more likely to be NO_x-limited. FNR_{SAT} was corrected based on the hourly surface FNR and O_3 data to make it better to reflect O_3 formation in a day. After correcting FNR_{SAT} with seasonal correction coefficients of 0.85, 0.84, and 0.77 for spring, summer, and autumn respectively, O_3 formation regime in Shanghai was more inclined to VOC-limited in both time and spatial distribution, and the effectiveness of FNR_{SAT} correction was confirmed by the surface observation.~~was closer to the observation result of LP-DOAS.~~ Thus, this correction is significant for using satellite data to improve the accuracy in indicating surface O_3 formation.

Data availability. Data are available for scientific purposes upon request to the corresponding author.

Author Contributions: DL and SW designed and implemented the research, and prepared the manuscript; RX contributed to the analysis of OMI products and MEIC inventory; JZ provided the HCHO and NO_2 data observed by LP-DOAS; SZ and ZS revised the manuscript; BZ provided constructive comments and supported the DOAS measurements.

Competing interests. The authors declare that they have no conflict of interest.

Acknowledgments: We acknowledge the free use of OMI HCHO and NO_2 products from NASA Goddard Earth Sciences (GES) Data and Information Services Center (DISC). We also thank Center for Earth System Science, Tsinghua University for MEIC data.

Financial support: This research was funded by National Key Research and Development Program of China (2017YFC0210002), National Natural Science Foundation of China (41775113, 21777026), and Funds for International Cooperation and Exchange of the National Natural Science Foundation of China (Grant No. 42061134006).

References

An, J. Y., Huang, Y. W., Huang, C., Wang, X., Yan, R. S., Wang, Q., Wang, H. L., Jing, S. A., Zhang, Y., Liu, Y. M., Chen, Y., Xu, C., Qiao, L. P., Zhou, M., Zhu, S. H., Hu, Q. Y., Lu, J., and Chen, C. H.: Emission inventory of air pollutants and chemical speciation for specific anthropogenic sources based on local measurements in the Yangtze River Delta region, China, Atmos Chem Phys, 21, 2003-2025, https://doi.org/10.5194/acp-21-2003-2021, 2021.

Bovensmann, H., Burrows, J. P., Buchwitz, M., Frerick, J., Noel, S., Rozanov, V. V., Chance, K. V., and Goede, A. P. H.: SCIAMACHY: Mission objectives and measurement modes, J Atmos Sci, 56, 127-150, https://doi.org/Doi 10.1175/1520-0469(1999)056<0127:Smoamm>2.0.Co;2, 1999.

Burrows, J. P., Weber, M., Buchwitz, M., Rozanov, V., Ladstatter-Weissenmayer, A., Richter, A., DeBeek, R., Hoogen, R., Bramstedt, K., Eichmann, K. U., and Eisinger, M.: The global ozone monitoring experiment (GOME): Mission concept and first scientific results, J Atmos Sci, 56, 151-175, https://doi.org/Doi 10.1175/1520-0469(1999)056<0151:Tgomeg>2.0.Co;2, 1999.

Callies, J., Corpaccioli, E., Eisinger, M., Hahne, A., and Lefebvre, A.: GOME-2 - Metop's second-generation sensor for operational ozone monitoring, Esa Bull-Eur Space, 28-36, 2000.

Chan, K. L., Wang, Z. R., Ding, A. J., Heue, K. P., Shen, Y. C., Wang, J., Zhang, F., Shi, Y. N., Hao, N., and Wenig, M.: MAX-DOAS measurements of tropospheric NO_2 and HCHO in Nanjing and a comparison to ozone monitoring instrument observations, Atmos Chem Phys, 19, 10051-10071, https://doi.org/10.5194/acp-19-10051-2019, 2019.

~~Chi, X. Y., Liu, C., Xie, Z. Q., Fan, G. Q., Wang, Y., He, P. Z., Fan, S. D., Hong, Q. Q., Wang, Z., Yu, X. W., Yue, F. E., Duan, J. B., Zhang, P. F., and Liu, J. G.: Observations of ozone vertical profiles and corresponding precursors in the low troposphere in Beijing, China, Atmos Res, 213, 224-235, https://doi.org/10.1016/j.atmosres.2018.06.012, 2018.~~

De Smedt, I., Van Roozendael, M., Stavrakou, T., Muller, J. F., Lerot, C., Theys, N., Valks, P., Hao, N., and van der A, R.: Improved retrieval of global tropospheric formaldehyde columns from GOME-2/MetOp-A addressing noise reduction and instrumental degradation issues, Atmos Meas Tech, 5, 2933-2949, https://doi.org/10.5194/amt-5-2933-2012, 2012.

Duncan, B. N., Yoshida, Y., Damon, M. R., Douglass, A. R., and Witte, J. C.: Temperature dependence of factors controlling isoprene emissions, Geophys Res Lett, 36, https://doi.org/10.1029/2008GL037090, 2009.

Duncan, B. N., Yoshida, Y., Olson, J. R., Sillman, S., Martin, R. V., Lamsal, L., Hu, Y. T., Pickering, K. E., Retscher, C., Allen, D. J., and Crawford, J. H.: Application of OMI observations to a space-based indicator of NO_x and VOC controls on surface ozone formation, Atmos Environ, 44, 2213-2223, https://doi.org/10.1016/j.atmosenv.2010.03.010, 2010.

Fan, J. C., Ju, T. Z., Wang, Q. H., Gao, H. Y., Huang, R. R., and Duan, J. L.: Spatiotemporal variations and potential sources of tropospheric formaldehyde over eastern China based on OMI satellite data, Atmos Pollut Res, 12, 272-285, https://doi.org/10.1016/j.apr.2020.09.011, 2021.

Gao, W., Tie, X. X., Xu, J. M., Huang, R. J., Mao, X. Q., Zhou, G. Q., and Chang, L. Y.: Long-term trend of O_3 in a mega City (Shanghai), China: Characteristics, causes, and interactions with precursors, Sci Total Environ, 603, 425-433, https://doi.org/10.1016/j.scitotenv.2017.06.099, 2017.

Geng, F. H., Tie, X. X., Xu, J. M., Zhou, G. Q., Peng, L., Gao, W., Tang, X., and Zhao, C. S.: Characterizations of ozone, NO_x, and VOCs measured in Shanghai, China, Atmos Environ, 42, 6873-6883, https://doi.org/10.1016/j.atmosenv.2008.05.045, 2008.

Jin, X. M., and Holloway, T.: Spatial and temporal variability of ozone sensitivity over China observed from the Ozone Monitoring Instrument, J. Geophys. Res.-Atmos., 120, 7229-7246, https://doi.org/10.1002/2015jd023250, 2015.

Jin, X. M., Fiore, A. M., Murray, L. T., Valin, L. C., Lamsal, L. N., Duncan, B., Folkert Boersma, K., De Smedt, I., Abad, G. G., Chance, K., and Tonnesen, G. S.: Evaluating a Space-Based Indicator of Surface Ozone-NO_x-VOC Sensitivity Over Midlatitude Source Regions and Application to Decadal Trends, J. Geophys. Res.-Atmos., 122, 10231-10253, https://doi.org/10.1002/2017jd026720, 2017.

Jin, X. M., Fiore, A., Boersma, K. F., De Smedt, I., and Valin, L.: Inferring Changes in Summertime Surface Ozone-NO_x-VOC Chemistry over US Urban Areas from Two Decades of Satellite and Ground-Based Observations, Environ Sci Technol, 54, 6518-6529, https://doi.org/10.1021/acs.est.9b07785, 2020.

Krotkov, N. A., McLinden, C. A., Li, C., Lamsal, L. N., Celarier, E. A., Marchenko, S. V., Swartz, W. H., Bucsela, E. J., Joiner, J., Duncan, B. N., Boersma, K. F., Veefkind, J. P., Levelt, P. F., Fioletov, V. E., Dickerson, R. R., He, H., Lu, Z. F., and Streets, D. G.: Aura OMI observations of regional SO_2 and NO_2 pollution changes from 2005 to 2015, Atmos Chem Phys, 16, 4605-4629, https://doi.org/10.5194/acp-16-4605-2016, 2016.

Lee, H., Ryu, J., Irie, H., Jang, S. H., Park, J., Choi, W., and Hong, H.: Investigations of the Diurnal Variation of Vertical HCHO Profiles Based on MAX-DOAS Measurements in Beijing: Comparisons with OMI Vertical Column Data, Atmosphere-Basel, 6, 1816-1832, https://doi.org/10.3390/atmos6111816, 2015.

Levelt, P. F., Van den Oord, G. H. J., Dobber, M. R., Malkki, A., Visser, H., de Vries, J., Stammes, P., Lundell, J. O. V., and Saari, H.: The Ozone Monitoring Instrument, Ieee T Geosci Remote, 44, 1093-1101, https://doi.org/10.1109/Tgrs.2006.872333, 2006.

Li, K., Jacob, D. J., Liao, H., Shen, L., Zhang, Q., and Bates, K. H.: Anthropogenic drivers of 2013-2017 trends in summer surface ozone in China, P Natl Acad Sci USA, 116, 422-427, https://doi.org/10.1073/pnas.1812168116, 2019.

Li, X., Rohrer, F., Brauers, T., Hofzumahaus, A., Lu, K., Shao, M., Zhang, Y. H., and Wahner, A.: Modeling of HCHO and CHOCHO at a semi-rural site in southern China during the PRIDE-PRD2006 campaign, Atmos Chem Phys, 14, 12291-12305, https://doi.org/10.5194/acp-14-12291-2014, 2014.

Ling, Z. H., Guo, H., Chen, G. X., Lam, S. H. M., and Fan, S. J.: Formaldehyde and Acetaldehyde at Different Elevations in Mountainous Areas in Hong Kong, Aerosol Air Qual Res, 16, 1868-1878, https://doi.org/10.4209/aaqr.2015.09.0571, 2016.

Liu, H. R., Liu, C., Xie, Z. Q., Li, Y., Huang, X., Wang, S. S., Xu, J., and Xie, P. H.: A paradox for air pollution controlling in China revealed by "APEC Blue" and "Parade Blue", Sci Rep-Uk, 6, 13, https://doi.org/10.1038/srep34408, 2016.

Liu, R., Feng, T., Wang, S. S., Shi, C. Z., Guo, Y. L., Nan, J. L., Deng, Y., and Zhou, B.: OMI satellite observed formaldehyde column from 2006 to 2015 over Xishuangbanna, southwest China, and validation using ground based zenith-sky DOAS, Sci Total Environ, 613, 168-175, https://doi.org/10.1016/j.scitotenv.2017.08.210, 2018a.

Liu, Y., Li, L., An, J., Zhang, W., Yan, R., Huang, L., Huang, C., Wang, H., Wang, Q., and Wang, M.: Emissions, Chemical Composition, and Spatial and Temporal Allocation of the BVOCs in the Yangtze River Delta Region in 2014, ENVIRONMENTAL SCIENCE, 39, 608-617, 2018b.

Liu, Y., Li, L., An, J. Y., Huang, L., Yan, R. S., Huang, C., Wang, H. L., Wang, Q., Wang, M., and Zhang, W.: Estimation of biogenic VOC emissions and its impact on ozone formation over the Yangtze River Delta region, China, Atmos Environ, 186, 113-128, https://doi.org/10.1016/j.atmosenv.2018.05.027, 2018c.

Liu, Y., Tang, Z. P., Abera, T., Zhang, X. Z., Hakola, H., Pellikka, P., and Maeda, E.: Spatio-temporal distribution and source partitioning of formaldehyde over Ethiopia and Kenya, Atmos Environ, 237, 9, https://doi.org/10.1016/j.atmosenv.2020.117706, 2020.

Luo, H. H., Yang, L. F., Yuan, Z. B., Zhao, K. H., Zhang, S., Duan, Y. S., Huang, R. Z., and Fu, Q. Y.: Synoptic condition-driven summertime ozone formation regime in Shanghai and the implication for dynamic ozone control strategies, Sci Total Environ, 745, 12, https://doi.org/10.1016/j.scitotenv.2020.141130, 2020.

Marais, E. A., Jacob, D. J., Kurosu, T. P., Chance, K., Murphy, J. G., Reeves, C., Mills, G., Casadio, S., Millet, D. B., Barkley, M. P., Paulot, F., and Mao, J.: Isoprene emissions in Africa inferred from OMI observations of formaldehyde columns, Atmos Chem Phys, 12, 6219-6235, https://doi.org/10.5194/acp-12-6219-2012, 2012.

Martin, R. V., Fiore, A. M., and Van Donkelaar, A.: Space-based diagnosis of surface ozone sensitivity to anthropogenic emissions, Geophys Res Lett, 31, L06120 06121-06124, https://doi.org/10.1029/2004gl019416, 2004a.

Martin, R. V., Parrish, D. D., Ryerson, T. B., Nicks, D. K., Chance, K., Kurosu, T. P., Jacob, D. J., Sturges, E. D., Fried, A., and Wert, B. P.: Evaluation of GOME satellite measurements of tropospheric NO_2 and HCHO using regional data from aircraft campaigns in the southeastern United States, J. Geophys. Res.-Atmos., 109, 11, https://doi.org/10.1029/2004jd004869, 2004b.

Miller, C. C., Jacob, D. J., Marais, E. A., Yu, K. R., Travis, K. R., Kim, P. S., Fisher, J. A., Zhu, L., Wolfe, G. M., Hanisco, T. F., Keutsch, F. N., Kaiser, J., Min, K. E., Brown, S. S., Washenfelder, R. A., Abad, G. G., and Chance, K.: Glyoxal yield from isoprene oxidation and relation to formaldehyde: chemical mechanism, constraints from SENEX aircraft observations, and interpretation of OMI satellite data, Atmos Chem Phys, 17, 8725-8738, https://doi.org/10.5194/acp-17-8725-2017, 2017.

Millet, D. B., Jacob, D. J., Boersma, K. F., Fu, T. M., Kurosu, T. P., Chance, K., Heald, C. L., and Guenther, A.: Spatial distribution of isoprene emissions from North America derived from formaldehyde column measurements by the OMI satellite sensor, J. Geophys. Res.-Atmos., 113, 18, https://doi.org/10.1029/2007jd008950, 2008.

Narumi, D., Kondo, A., and Shimoda, Y.: The effect of the increase in urban temperature on the concentration of photochemical oxidants, Atmos Environ, 43, 2348-2359, https://doi.org/10.1016/j.atmosenv.2009.01.028, 2009.

Palmer, P. I., Abbot, D. S., Fu, T. M., Jacob, D. J., Chance, K., Kurosu, T. P., Guenther, A., Wiedinmyer, C., Stanton, J. C., Pilling, M. J., Pressley, S. N., Lamb, B., and Sumner, A. L.: Quantifying the seasonal and interannual variability of North American isoprene emissions using satellite observations of the formaldehyde column, J. Geophys. Res.-Atmos., 111, 14, https://doi.org/10.1029/2005jd006689, 2006.

Pang, X. B., Mu, Y. J., Lee, X. Q., Zhang, Y. J., and Xu, Z.: Influences of characteristic meteorological conditions on atmospheric carbonyls in Beijing, China, Atmos Res, 93, 913-919, https://doi.org/10.1016/j.atmosres.2009.05.001, 2009.

Schroeder, J. R., Crawford, J. H., Fried, A., Walega, J., Weinheimer, A., Wisthaler, A., Muller, M., Mikoviny, T., Chen, G., Shook, M., Blake, D. R., and Tonnesen, G. S.: New insights into the column CH_2O/NO_2 ratio as an indicator of near-surface ozone sensitivity, J. Geophys. Res.-Atmos., 122, 8885-8907, https://doi.org/10.1002/2017jd026781, 2017.

Sharkey, T. D., and Loreto, F.: Water-stress, temperature, and light effects on the capacity for isoprene emission and photosynthesis of kudzu leaves, Oecologia, 95, 328-333, https://doi.org/10.1007/bf00320984, 1993.

Shen, L., Jacob, D. J., Zhu, L., Zhang, Q., Zheng, B., Sulprizio, M. P., Li, K., De Smedt, I., Abad, G. G., Cao, H. S., Fu, T. M., and Liao, H.: The 2005-2016 Trends of Formaldehyde Columns Over China Observed by Satellites: Increasing Anthropogenic Emissions of Volatile Organic Compounds and Decreasing Agricultural Fire Emissions, Geophys Res Lett, 46, 4468-4475, https://doi.org/10.1029/2019gl082172, 2019.

Sillman, S.: The use of NO_y, H_2O_2, and HNO_3 as indicators for Ozone-NO_x-Hydrocarbon sensitivity in Urban Locations, J. Geophys. Res.-Atmos., 100, 14175-14188, https://doi.org/doi 10.1029/94jd02953, 1995.

Souri, A. H., Choi, Y., Jeon, W., Woo, J. H., Zhang, Q., and Kurokawa, J.: Remote sensing evidence of decadal changes in major tropospheric ozone precursors over East Asia, J. Geophys. Res.-Atmos., 122, 2474-2492, https://doi.org/10.1002/2016jd025663, 2017.

Stavrakou, T., Muller, J. F., De Smedt, I., Van Roozendael, M., van der Werf, G. R., Giglio, L., and Guenther, A.: Global emissions of non-methane hydrocarbons deduced from SCIAMACHY formaldehyde columns through 2003-2006, Atmos Chem Phys, 9, 3663-3679, https://doi.org/10.5194/acp-9-3663-2009, 2009.

~~Su, W. J., Liu, C., Hu, Q. H., Fan, G. Q., Xie, Z. Q., Huang, X., Zhang, T. S., Chen, Z. Y., Dong, Y. S., Ji, X. G., Liu, H. R., Wang, Z., and Liu, J. G.: Characterization of ozone in the lower troposphere during the 2016 G20 conference in Hangzhou, Sci Rep-Uk, 7, 11, https://doi.org/10.1038/s41598-017-17646-x, 2017.~~

Su, W. J., Liu, C., Hu, Q. H., Zhao, S. H., Sun, Y. W., Wang, W., Zhu, Y. Z., Liu, J. G., and Kim, J.: Primary and secondary sources of ambient formaldehyde in the Yangtze River Delta based on Ozone Mapping and Profiler Suite (OMPS) observations, Atmos Chem Phys, 19, 6717-6736, https://doi.org/10.5194/acp-19-6717-2019, 2019.

Veefkind, J. P., Aben, I., McMullan, K., Forster, H., de Vries, J., Otter, G., Claas, J., Eskes, H. J., de Haan, J. F., Kleipool, Q., van Weele, M., Hasekamp, O., Hoogeveen, R., Landgraf, J., Snel, R., Tol, P., Ingmann, P., Voors, R., Kruizinga, B., Vink, R., Visser, H., and Levelt, P. F.: TROPOMI on the ESA Sentinel-5 Precursor: A GMES mission for global observations of the atmospheric composition for climate, air quality and ozone layer applications, Remote Sens Environ, 120, 70-83, https://doi.org/10.1016/j.rse.2011.09.027, 2012.

Vigouroux, C., Langerock, B., Aquino, C. A. B., Blumenstock, T., Cheng, Z. B., De Maziere, M., De Smedt, I., Grutter, M., Hannigan, J. W., Jones, N., Kivi, R., Loyola, D., Lutsch, E., Mahieu, E., Makarova, M., Metzger, J. M., Morino, I., Murata, I., Nagahama, T., Notholt, J., Ortega, I., Palm, M., Pinardi, G., Rohling, A., Smale, D., Stremme, W., Strong, K., Sussmann, R., Te, Y., van Roozendael, M., Wang, P. C., and Winkler, H.: TROPOMI-Sentinel-5 Precursor formaldehyde validation using an extensive network of ground-based Fourier-transform infrared stations, Atmos Meas Tech, 13, 3751-3767, https://doi.org/10.5194/amt-13-3751-2020, 2020.

Wang, T., Wang, P. C., Theys, N., Tong, D., Hendrick, F., Zhang, Q., and Van Roozendael, M.: Spatial and temporal changes in SO_2 regimes over China in the recent decade and the driving mechanism, Atmos Chem Phys, 18, 18063-18078, https://doi.org/10.5194/acp-18-18063-2018, 2018.

Wang, Y., Beirle, S., Lampel, J., Koukouli, M., De Smedt, I., Theys, N., Li, A., Wu, D. X., Xie, P. H., Liu, C., Van Roozendael, M., Stavrakou, T., Muller, J. F., and Wagner, T.: Validation of OMI, GOME-2A and GOME-2B tropospheric NO_2, SO_2 and HCHO products using MAX-DOAS observations from 2011 to 2014 in Wuxi, China: investigation of the effects of priori profiles and aerosols on the satellite products, Atmos Chem Phys, 17, 5007-5033, https://doi.org/10.5194/acp-17-5007-2017, 2017.

Wang, Y. P., Wang, Z. F., Yu, C., Zhu, S. Y., Cheng, L. X., Zhang, Y., and Chen, L. F.: Validation of OMI HCHO Products Using MAX-DOAS observations from 2010 to 2016 in Xianghe, Beijing: Investigation of the Effects of Aerosols on Satellite Products, Remote Sens-Basel, 11, 21, https://doi.org/10.3390/rs11020203, 2019.

Xing, C. Z., Liu, C., Hu, Q. H., Fu, Q. Y., Lin, H., Wang, S. T., Su, W. J., Wang, W. W., Javed, Z., and Liu, J. G.: Identifying the wintertime sources of volatile organic compounds (VOCs) from MAX-DOAS measured formaldehyde and glyoxal in Chongqing, southwest China, Sci Total Environ, 715, 12, https://doi.org/10.1016/j.scitotenv.2019.136258, 2020.

Xu, J. M., Tie, X. X., Gao, W., Lin, Y. F., and Fu, Q. Y.: Measurement and model analyses of the ozone variation during 2006 to 2015 and its response to emission change in megacity Shanghai, China, Atmos Chem Phys, 19, 9017-9035, https://doi.org/10.5194/acp-19-9017-2019, 2019.

Xue, R. B., Wang, S. S., Li, D. R., Zou, Z., Chan, K. L., Valks, P., Saiz-Lopez, A., and Zhou, B.: Spatio-temporal variations in NO_2 and SO_2 over Shanghai and Chongming Eco-Island measured by Ozone Monitoring Instrument (OMI) during 2008-2017, J Clean Prod, 258, 14, https://doi.org/10.1016/j.jclepro.2020.120563, 2020.

Zaveri, R. A., Berkowitz, C. M., Kleinman, L. I., Springston, S. R., Doskey, P. V., Lonneman, W. A., and Spicer, C. W.: Ozone production efficiency and NO_x depletion in an urban plume: Interpretation of field observations and implications for evaluating O_3-NO_x-VOC sensitivity, J. Geophys. Res.-Atmos., 108, 23, https://doi.org/10.1029/2002jd003144, 2003.

Zhang, C. X., Liu, C., Hu, Q. H., Cai, Z. N., Su, W. J., Xia, C. Z., Zhu, Y. Z., Wang, S. W., and Liu, J. G.: Satellite UV-Vis spectroscopy: implications for air quality trends and their driving forces in China during 2005-2017, Light-Sci Appl, 8, 12, https://doi.org/10.1038/s41377-019-0210-6, 2019.

Zhang, K., Li, L., Huang, L., Wang, Y. J., Huo, J. T., Duan, Y. S., Wang, Y. H., and Fu, Q. Y.: The impact of volatile organic compounds on ozone formation in the suburban area of Shanghai, Atmos Environ, 232, 11, https://doi.org/10.1016/j.atmosenv.2020.117511, 2020.

Zhang, K., Huang, L., Li, Q., Huo, J. T., Duan, Y. S., Wang, Y. H., Yaluk, E., Wang, Y. J., Fu, Q. Y., and Li, L.: Explicit modeling of isoprene chemical processing in polluted air masses in suburban areas of the Yangtze River Delta region: radical cycling and formation of ozone and formaldehyde, Atmos Chem Phys, 21, 5905-5917, https://doi.org/10.5194/acp-21-5905-2021, 2021.

Zhang, Q., Streets, D. G., He, K., Wang, Y., Richter, A., Burrows, J. P., Uno, I., Jang, C. J., Chen, D., Yao, Z., and Lei, Y.: NO_x emission trends for China, 1995-2004: The view from the ground and the view from space, J. Geophys. Res.-Atmos., 112, 18, https://doi.org/10.1029/2007jd008684, 2007.

Zhu, L., Jacob, D. J., Keutsch, F. N., Mickley, L. J., Scheffe, R., Strum, M., Abad, G. G., Chance, K., Yang, K., Rappengluck, B., Millet, D. B., Baasandorj, M., Jaegle, L., and Shah, V.: Formaldehyde (HCHO) As a Hazardous Air Pollutant: Mapping Surface Air Concentrations from Satellite and Inferring Cancer Risks in the United States, Environ Sci Technol, 51, 5650-5657, https://doi.org/10.1021/acs.est.7b01356, 2017a.

Zhu, L., Mickley, L. J., Jacob, D. J., Marais, E. A., Sheng, J. X., Hu, L., Abad, G. G., and Chance, K.: Long-term (2005-2014) trends in formaldehyde (HCHO) columns across North America as seen by the OMI satellite instrument: Evidence of changing emissions of volatile organic compounds, Geophys Res Lett, 44, 7079-7086, https://doi.org/10.1002/2017gl073859, 2017b.